The unique dual targeting of AGO1 by two types of PRMT enzymes promotes phasiRNA loading in Arabidopsis thaliana

Clément Barre-Villeneuve, Michèle Laudié, Marie-Christine Carpentier, Lauriane Kuhn, Thierry Lagrange, Jacinthe Azevedo-Favory

Nucleic Acids Research, 2024, 1–18
https://doi.org/10.1093/nar/gkae045
Molecular Biology

The unique dual targeting of AGO1 by two types of PRMT enzymes promotes phasiRNA loading in *Arabidopsis thaliana*

Clément Barre-Villeneuve[1,2], Michèle Laudié[1,2], Marie-Christine Carpentier[1,2], Lauriane Kuhn[3,4], Thierry Lagrange[1,2] and Jacinthe Azevedo-Favory[1,2,*]

[1]CNRS, Laboratoire Génome et Développement des Plantes, UMR 5096, 66860 Perpignan, France
[2]Université Perpignan Via Domitia, Laboratoire Génome et Développement des Plantes, UMR 5096, F-66860 Perpignan, France
[3]Plateforme protéomique Strasbourg – Esplanade, CNRS FR1589, Université de Strasbourg, IBMC, 2 allée Konrad Roentgen, F-67084 Strasbourg, France
[4]Fédération de Recherche CNRS FR1589, France
[*]To whom correspondence should be addressed. Tel: +33 4 30 19 81 22; Fax: +33 4 68 66 84 99; Email: jacinthe.azevedo-favory@univ-perp.fr

Abstract

Arginine/R methylation (R-met) of proteins is a widespread post-translational modification (PTM), deposited by a family of protein arginine/R methyl transferase enzymes (PRMT). Regulations by R-met are involved in key biological processes deeply studied in metazoan. Among those, post-transcriptional gene silencing (PTGS) can be regulated by R-met in animals and in plants. It mainly contributes to safeguard processes as protection of genome integrity in germlines through the regulation of piRNA pathway in metazoan, or response to bacterial infection through the control of AGO2 in plants. So far, only PRMT5 has been identified as the AGO/PIWI R-met writer in higher eukaryotes. We uncovered that AGO1, the main PTGS effector regulating plant development, contains unique R-met features among the AGO/PIWI superfamily, and outstanding in eukaryotes. Indeed, AGO1 contains both symmetric (sDMA) and asymmetric (aDMA) R-dimethylations and is dually targeted by PRMT5 and by another type I PRMT in *Arabidopsis thaliana*. We showed also that loss of sDMA didn't compromise AtAGO1 subcellular trafficking *in planta*. Interestingly, we underscored that AtPRMT5 specifically promotes the loading of phasiRNA in AtAGO1. All our observations bring to consider this dual regulation of AtAGO1 in plant development and response to environment, and pinpoint the complexity of AGO1 post-translational regulation.

Graphical abstract

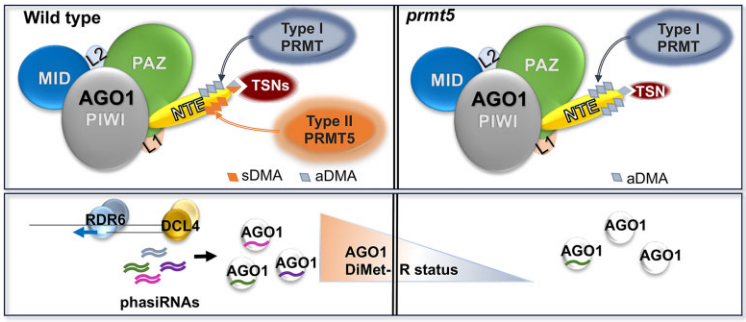

Introduction

Plants have evolved sophisticated and specialized RNA silencing pathways that fine-tune their development in response to environment, but also contribute to plant immunity and genome integrity (1–4). These processes ensure sequence specific gene silencing mediated by the action of Argonaute effector proteins (AGO) guided by small RNAs (sRNA), which can target DNA to silence transcription (Transcriptional Gene Silencing, TGS) or mRNA to trigger transcript degradation or translational inhibition (Post-Transcriptional Gene Silencing, PTGS). In Arabidopsis, AGO1 is the main effector of PTGS, leading to miRNA- or tasi/phasiRNA-dependent repression of genes involved in development such as phase transitions, patterning, cell fate and hormone regulations. In addition, AGO1 action contributes to plant immunity (5,6) and abiotic stress responses (7,8). A null *ago1* mutant exhibits very severe growing phenotypes and is self-sterile. To another extent, hypomorphic mutants show various defects in floral organ and leaf development, in phyllotaxy, stem cell maintenance and fertility (9,10). On the other way, the overexpres-

Received: July 6, 2023. **Revised:** December 18, 2023. **Editorial Decision:** January 5, 2024. **Accepted:** January 12, 2024

sion of AGO1 can also trigger deleterious effects (asymmetric rosette leaf formation, curled or twisted leaves, sterility) (11). Consequently, a tight control of AGO1 expression and activity remains crucial (12). To do this, AGO1 homeostasis is post-transcriptionally regulated through a well described miR168-mediated negative feedback loop (11,13) and AGO1 protein turnover is controlled by autophagy (14–17). In this context, another mean to modulate the activity of such key regulators relies on post-translational modifications (PTMs). Little is known so far about the regulation of AGO1 activity through PTM in plants. Recent evidences have highlighted that some effectors from the AGO/PIWI superfamily are regulated by Protein arginine/R Methyl Transferase 5 (PRMT5) enzyme. PRMT5 belongs to the highly conserved PRMT family, classified into three groups according to the nature of the modification deposited on the side chain of the arginine/R residue, i.e. monomethylarginine/MMA (Type III), asymmetric dimethylarginine/aDMA (Type I), and symmetric dimethylarginine/sDMA (Type II). *A. thaliana* genome encode 9 PRMTs, and among those, PRMT5 is the only type II enzyme conserved in both metazoan and plants that deposits sDMA marks preferentially in RGG/GRG sequence contexts. In metazoans, PRMT5 regulates the germline specific PIWI, Aub and AGO3 effectors involved in the silencing of transposons (TE) (18–20). Once methylated, these RGG/GRG motifs are recognized by a TUDOR domain-containing reader protein. This association contributes to the quality control of the piRNA production pathway, therefore protecting the primordia germ cell from TE expression that can lead to defects in cell specification and gametogenesis. Hu and collaborators (21) have shown more recently that AGO2, one of the main PTGS effectors in plant immunity, is modified by PRMT5 in *A. thaliana*, and that AtPRMT5 and AtTudor-SN proteins (TSN) lower its small RNA loading capacity. Indeed, the sDMA-AGO2 form is more prone to degradation and its association with AtTSN proteins also promotes the degradation of the loaded sRNA. This mode of regulation of AtAGO2 is especially interesting in the context of *Pseudomonas syringae* infection which inhibits the expression of *AtPRMT5*, and thereby promotes AtAGO2 activity to restrict bacterial invasion (21). The RGG/GRG motifs repeats identified in all these studies are concentrated in the N-terminal regions of AGO/PIWI proteins. Such clusters are also present in the N-terminal extension of AtAGO1 (NTE, from 1 to 189 aa). The function of this extension is still elusive compared to what is known for the other domains of AtAGO1. This region contains NLS and NES sequences which allow AtAGO1 to shuttle between nucleus to load miRNAs, and cytoplasm to regulate corresponding miRNA targets (22). Moreover, a linear N-coil peptide (F177-K190), located just upstream of the ArgoN domain, is essential for AGO1 dependent miRNA function in *A. thaliana* (17,23,24). Consequently, the presence of RGG/GRG motifs in such an environment prompted us to address the potential role of PRMT5 on AGO1 activity in *A. thaliana*.

In this study, we highlight that RGG/GRG motifs are also present in the NTE of some AGO proteins involved in PTGS in Arabidopsis i.e. AtAGO1, AtAGO2, AtAGO3 and AtAGO5, and are also widely found in AGO1 plant orthologs. These sequences are mainly clustered, in a region called here Nt-AGO-RGG/GRG and located in predicted intrinsically disordered domains (IDR). Then, we have shown that AtAGO1 is symmetrically dimethylated by AtPRMT5 *in vivo*, and surprisingly also contains aDMA residues in its Nt-AtAGO1-RGG/GRG region, thus revealing that AtAGO1 is also modified by a type I PRMT. Then, we have assessed more specifically the contribution of PRMT5 to various aspects of AtAGO1 activity. We have demonstrated that AtAGO1 and AtTSN proteins interacts together, however this association does not rely exclusively on the presence of sDMA marks. We have also concluded that AtAGO1 subcellular trafficking is not impaired in *atprmt5* mutants. In the framework of this last question, we have interestingly uncovered that AtAGO1 can relocate to cytoplasmic discrete foci in response to heat stress (HS), but still independently of it sDMA status. We have shown that AtPRMT5 dependent regulation does not impact the accumulation of AtAGO1, but specifically promotes the loading of a subset of phasiRNA in AtAGO1. Finally, all our observations emphasize the amazing complexity of AGO1 regulation by R-met and raise the underneath questions of PRMTs functional redundancy, specificity, competition, or hierarchy for AGO1 access and control in *A. thaliana*.

Materials and methods

Plant material

Arabidopsis thaliana cv Columbia-0 and *prmt5* mutants in Columbia background (previously described *prmt5-2 and prmt5-4* alleles corresponding respectively to Salk095085 and Salk073624, and a new *prmt5-6* allele from SAIL852H03 mutant) were used in this study. The *pSUC2-amiRSUL* line was provided by Dr F. Brioudes (25). The *pAGO1:GFP-AGO1/ago1-3* line was provided by Dr N. Bologna (22). The *tsn1,tsn2* double mutant in Columbia background is obtained by crossing two new mutant alleles *tsn1-5* (GK393H06) and *tsn2-3* (SALK073041).

Plants were either grown in soil or cultivated *in vitro* on plates containing half Murashige and Skoog medium (Duchefa; 2.20 g/l); 0.5g/l MES, pH 5.7, and 7 g/l agar. For *in vitro* experiments, seeds were incubated for 48 h at 6°C in the dark prior incubation in growth chambers and cultivated at 20°C, 60–75% hygrometry with a 16-h light/8-h dark photoperiod (100 μE m^{-2} s^{-1} light LED light from Vegeled). For *in vitro* culture, the seeds were surface-sterilized before been sown on plates, stratified for 48 h at 6°C in the dark, and then grown in a chamber at 20°C, under 120 μE m^{-2} s^{-1} light (LEDs with white 4500 K spectrum, from Vegeled) regulated in a 16-h-light/8-h-dark cycle.

Plant treatments

For leptomycin b treatment, five-day-old seedlings grown *in vitro* on solid 1/2 MS agar medium were transferred to 1/2 MS liquid medium. After 2 days of acclimatisation *in vitro* in this medium, the seedlings were then incubated for 12–24 h, in the presence of 2.5 μM of leptomycin b (SIGMA) or ethanol (mock control) before observations with confocal microscope

For the heat-stress experiments, five-day-old seedlings grown *in vitro* on solid half-MS medium were exposed to a heat stress at 37°C for 15 min in a confined cabinet between slide and coverslip. After this treatment, they were directly observed with confocal microscope.

Confocal microscopy imaging

The apex from *GFP-AGO1/ago1-3/prmt5-1* or *GFP-AGO1/ago1-3* roots of 5–7-day-old seedlings grown *in vitro* were used to monitor the subcellular distribution of GFP-

AGO1 fusion protein. Observations and acquisitions were performed using LSM700 (Zeiss) confocal microscope with the following excitation and emission wavelengths: GFP: 488 nm/490–540 nm; YFP: 488 nm/490–540 nm; RFP: 555 nm.

Sequence conservation and bio-informatic structure predictions of Argonaute proteins

For the alignment of Argonaute proteins, the AGO1, AGO2, AGO3 and AGO5 protein sequences were obtained from the TAIR10 Genome accessible on Phytozome v12.1. The alignment was done thanks to the MEGAX software using ClustalW set as follows: Gap Opening Penalty for Multiple and Pairwise Alignment: 10, Gap Extension Penalty for Multiple Alignment: 0.20, Gap Extension Penalty for Pairwise Alignment: 0.10, Protein Weight Matrix: Gonnet, Residue-specific Penalties: ON, Hydrophilic Penalties: ON, Gap Separation Matrix: 4; End Gap Separation: OFF, Use Negative Matrix: OFF, Delay Divergent Cutoff: 30%. The alignment was visualized thanks to Boxshade server with the 'Fraction of sequences' parameter set on 0.5.

The protein sequences of AtAGO1 homologs were obtained after a BLAST on the TAIR10 Genome accessible on Phytozome v12.1, with the AtAGO1 protein sequence as input. For each species, one, two or three of the first sequences with the best score are selected for the alignment. The alignment was done through the MultiAlin website (http://multalin.toulouse.inra.fr/multalin/multalin.html) with the default parameters, except for the low consensus value which was set at 40% instead of 50%.

The predicted 3D structure of AtAGO1 was obtained from AlphaFold protein structure database (https://alphafold.ebi.ac.uk/ prediction; (26). The protein structure obtained was then treated with UCSF Chimera, production version 1.15 (build 42258) to visualize the different domains and amino acids of interest.

The prediction of long intrinsically disordered unstructured regions and protein binding motifs in disordered protein regions forAtAGO1 was done using ANCHOR2 in IUPRED3 (https://iupred.elte.hu/).

Picture analyses

The chlorosis phenotype of the plants in the *amiRSUL* background were analysed thanks to ImageJ 1.53k (Wayne Rasband and contributors; National Institutes of Health, USA). To perform this analysis, first, we set the picture scale. Then, we used the Image/Adjust/Color Threshold function to select the chlorotic area of each rosette leaf, or to select the whole leaf surface of each leaf. We used the Color Threshold parameters to correctly visualise the chlorotic area on all rosette leaves surfaces for all lines. After selection of the chlorotic area or the whole leaf area for each leaf, the pictures were binarised to get a black and white picture. Then, we removed, in the pictures with the selected whole leaves area, all outliners which are not part of the leaves area. Finally, we used the Analyze/Set Measurements tool to measure the integrated density of the chlorotic veins of each leaf or of the whole surface of each leaf. The integrated density corresponds to the average pixel intensity on the surface, and as the picture has been binarised only the surface change between each leaf for the whole leaf area or the chlorotic veins area. Then we measured the integrated density for the whole leaf area and the chlorotic vein area; and we calculated the percentage of chlorotic area on the whole leaf surface.

Total protein extractions and immunodetections

Plant samples were harvested and ground in liquid nitrogen, and total proteins were extracted using following methods depending on the question addressed. Thus, total crude extracts were obtained using Laemmli extraction (2 volumes of Laemmli buffer/1 volume of grinded tissue); total purified proteins (including insoluble ones) were extracted using a protocol adapted from Hurkman and Tanaka (27); and finally, soluble proteins fractions were prepared according to the description provided in the next 'immunoprecipitations' part. Total purified proteins were then quantified using Brafdord method (Bio-Rad protein assay). Before SDS-PAGE, Laemmli buffer was added and coomassie staining was used to calibrate loadings if needed. For western blots, proteins were separated on SDS-PAGE gels and blotted onto Immobilon-P PVDF membrane (Cat. No. IPVH00010; MerckMillipore). Protein blot analyses were performed using either the Immobilon Western Chemiluminescent HRP Substrate (Merck Millipore) followed by Fusion Solo 6S edge image acquisition (Vilber Lourmat) or direct colorimetric detection on membrane (BCIP®/NBT-Purple liquid substrate system for membrane, SIGMA).

All the antibodies used in this study are listed in Supplementary Table S2.

Immunoprecipitations

The samples were frozen during harvesting and ground in liquid nitrogen to get a fine powder. They were homogenized in two volumes of cold extraction buffer (EB150: Tris–HCl 50 mM pH7.5; NaCl 150 mM; glycerol 10%; $MgCl_2$ 5 mM; NP40 0.2%; 1 anti-proteases tablets EDTA-free, from Roche/SIGMA,; MG132 10 μM) using a Dounce homogenizer (pestle type B). The inputs fractions were finally obtained after two centrifugations steps (30 min and 15 min at 21 000g, at 4°C). Immunoprecipitations were then performed either with AGO1 antibodies (from Agrisera or from Eurogentec, see Supplementary Table S2) or with Chromotek GFP-trap magnetic beads (Proteintech). For AGO1 IPs, the inputs were incubated with anti-AGO1 antibodies for 1–3 h (10 rpm, 4°C). The immunocomplexes were then immobilized with equilibrated dynabeads coupled to the protein A (Invitrogen) during 1 h (10 rpm, 4°C). The beads were then isolated and washed 5 times with EB150 buffer and once with PBS buffer. The protein complexes were eluted either directly for protein detection (western blot) or for small RNA extraction and protein detection simultaneously. In this last case, TRI-reagent (Invitrogen) was added to the beads and the separation of sRNA and proteins was achieved according to the supplier's instructions. Proteins were then precipitated by adding three volumes of acetone to phenolic phase. After an overnight incubation at -20°C, the proteins were sedimented by centrifugation (15 min, 21 000g, 4°C) and the pellets were washed with acetone 80% (v/v) prior to protein resuspension with 4x Laemmli buffer and denaturation.

For GFP IPs, the inputs were incubated with equilibrated GFP-trap magnetic beads for 1 h. The beads were then washed 6 times (5 washes with EB150 and 1 last wash with PBS). The proteins were finally eluted with glycine (0.1N, pH 2.5), and prepared for subsequent SDS-PAGE and western blots.

Samples preparation and mass spectrometry analysis (nanoLC–MS/MS)

Protein bands were excised from the SDS-PAGE gel and individually destained in 25mM ammonium bicarbonate containing 50% (v/v) acetonitrile. Proteins were further reduced with 10mM dithiothreitol (DTT) (45 min, 56°C) and alkylated with 55mM iodoacetamide (in the dark for 1 h at room temperature). 50 ng of modified sequencing-grade trypsin (Promega, Madison, WI) were added on gel pieces for digestion, overnight, at 37°C. Resulting peptides were extracted from the gel pieces (ultra-pure water containing 60% acetonitrile and 5% formic acid) and vacuum-dried in a SpeedVac concentrator.

Dried tryptic digests were re-suspended in 20 µl of water containing 0.1% (v/v) formic acid (solvent A). The peptide mixtures were analysed using an Easy-nanoLC-1000 system coupled to a Q-Exactive Plus mass spectrometer (Thermo-Fisher Scientific, Bremen, Germany) operating in positive mode with a nanoelectrospray source. 5 µl of each sample were loaded on a C-18 precolumn (75 µm ID × 20 mm nanoViper, 3 µm Acclaim PepMap; Thermo-Fisher Scientific) at 800 bars in solvent A. After desalting and concentration, the pre-column was switched online with the analytical C18 analytical column (75 µm ID × 25 cm nanoViper, 3µm Acclaim PepMap; Thermo-Fisher Scientific) equilibrated in solvent A: solvent B (95:5; v/v). Peptides were eluted at a flow rate of 300 nl/min using a gradient from 5% B to 20% B in 120 min, from 20% B to 32% B in 15min, from 32% B to 95% B in 1min and 95% B to 95% B during 24min. The Q-Exactive Plus was operated in data-dependent acquisition mode (DDA) with Xcalibur software (Thermo-Fisher Scientific). Survey MS scans were acquired at a resolution of 70K at 200 m/z (mass range 350–1250), with a maximum injection time at 100ms and an automatic gain control (AGC) set at 3e6. Up to 10 of the most intense multiply charged ions ($\geq$2) were selected for HCD fragmentation with a normalized collision energy set at 27, at 17.5K resolution, with a maximum injection time at 100ms and AGC set at 1e3. A dynamic exclusion time of 20 s was applied during the peak selection process. The mass spectrometric data were deposited to the ProteomeXchange Consortium via the PRIDE partner repository with the dataset identifier PXD043460 and 10.6019/PXD043460.

Database search and mass-spectrometry data post-processing

MS datasets generated by the mass spectrometer were searched against the TAIRv10 database with a decoy strategy (54563 protein forward sequences using Mascot algorithm (version 2.8, Matrix Science). The following parameters were set in Mascot: Trypsin/P and 3 missed cleavages for the enzyme; Acetyl(Protein-Nterm), Carbamidomethyl(Cys), Oxidation(Met) and Phosphorylation(Ser/Thr/Tyr) for the variable modifications; 10ppm for the peptide mass tolerance and 0.02Da for the fragment mass tolerance. The resulting .dat Mascot files were then imported into Proline v2.1 package (28) for further post-processing. Proteins were validated on Mascot pretty rank equal to 1, PSM (Peptide Spectrum Match) score above 25, and 1% FDR (False Discovery Rate) on both PSM and protein sets (based on score). Proteins were validated if they were identified by at least one proteotypic (unique) peptide and MS/MS fragmentation spectra were carefully inspected after the FDR validation, especially for modified peptides. To further characterize dimethylated residues, a second database search was performed with the same Mascot algorithm with the following parameters: a database containing AGO1 sequence and classical contaminants (keratins, trypsin, …), an increased enzyme specificity (semiTrypsin), Methyl(KR) and DiMethyl(KR) as additional variable modifications. The other Mascot parameters remained unchanged compared to the first round of database search. The MS/MS spectra matching on dimethylated peptides were then manually inspected to precisely confirm the localization of the modification. Furthermore, the score from each individual PSM (Peptide – Spectrum Match) was compared to the Mascot identity threshold: the PSM was finally validated if the related Mascot score was above the identity threshold ($P < 0.05$).

Spectral Count quantification was reinforced by the reconstruction of the chromatographic elution peaks from AGO1, TSN1 and TSN2 peptides (Extracted Ion Chromatogram or EIC quantification). Raw MS data were imported into Proteome Discoverer 2.4 software (Thermo-Fisher Scientific). A database search was first conducted with two different algorithms (Sequest and MS-Amanda) with the same parameters as those used for the Spectral Count quantification with Mascot algorithm, especially concerning the variable modifications. The EIC quantification was performed through the addition of the 'Precursor Ions quantifier' node to the post-processing workflow in Proteome Discoverer, with the following parameters: (i) unique and razor peptides, (ii) precursor abundance based on intensity, (iii) no normalization and no missing values imputation. The peptide abundance extraction was performed with a 5 ppm m/z tolerance and 60 s as retention time tolerance. The three best peptides were considered for each protein, based on the highest Sequest and MS-Amanda composite scores.

RNA extractions

Plant samples were harvested and ground in liquid nitrogen, and total RNA are extracted using either the RNeasy Plant Mini Kit (QIAGEN), or the TRI-reagent (MRC research) method. For both methods, the genomic DNA was digested using DNase I (Qiagen) directly on columns during the RNeasy Plant Mini Kit procedure or on total RNA obtained with tri-reagent. The DNase I enzyme was subsequently eliminated by the RNA clean-up step (RNeasy Plant Mini Kit) or by a phenol–chloroform extraction.

Small RNA extraction from input extracts and AGO1 IP (for sRNA-seq) were performed using TRI-reagent (Invitrogen). For AGO1 IPs, the TRI-reagent solution was added directly to the beads to elute and separate sRNA and proteins, and sRNA were precipitated according to supplier's instructions, in presence of 30 µg of Glycoblue (Invitrogen).

RT-qPCR

Between 500 ng to 2 µg of total RNA were reverse-transcribed into cDNA using the SuperScript®IV Reverse Transcriptase (ThermoFisher scientific) in the presence of a mix of random primers and oligodT_{18}. Then qPCRs were prepared using the PowerTrack Syber^{TM} Green Master Mix (AppliedBiosystems) and performed with the LightCycler®480 (Roche) programmed as follow: 95°C for 5 min, followed by

40 cycles of 95°C for 15 sec and 60°C for 1 min. To assess the melting curve of the primers, the samples were denatured at 95°C, and then cool to 60°C at 2.2°C/s. The fluorescence signal was collected continuously from 60 to 95°C at 0.04°C/sec. Finally, the samples were cooled at 40°C for 30 s. Quantifications were determined from a standard curve and results were normalized to *ACTIN7* or *GAPDH*.

All primers used in this work are listed in Supplementary Table S3.

Preparation and sequencing of the small RNA librairies

The preparation of sRNA libraries, their quality controls and sequencing were performed by FASTERIS company (Illumina TrueSeq small RNA library prep; Nextseq 500 instrument; 1 × 75 bp single-end reads sequencing; production of 11 × 10^6 to 22 × 10^6 reads corresponding to 18–26 nt-long sRNAs/library). All these experiments were performed starting from *A. thaliana* closed buds. The libraries for total small RNA populations were prepared from the inputs fractions used for AGO1 IPs. In this case, a polyacrylamide gel-sizing selection step (18–30 nt) was included prior to preparation of the libraries. The small RNAs loaded into AGO1, purified from the AGO1 IPs, were used directly to prepare the libraries.

Sequencing data are available on the Gene Expression Omnibus database as GSE236628.

Small RNA seq bio-informatic analysis

For each library, reads were trimmed using Trimmomatic v0.36 (29).

To identify the nature of small RNA, libraries (21, 22, 23, 24nt) were mapped against *Arabidopsis thaliana* mature miRNA from Mirdatabase with bowtie2.

In parallel, reads were mapped against TAIR10 genome with bowtie2 and custom parameters for small sequences (-D 5 -R 2 -N 1 -L 5). TAIR10 genome was divided in 100 pb windows with bedtools makewindows. Count for each 100pb bin was performed with bedtools coverage. Differential expression analyses were performed using the Bioconductor R package DESeq2 (30), with a false discovery rate of 0.05. *P* values were corrected for multiple tests by the Benjamini–Hochberg rule (adjusted *P* value).

The ChromoMap was drawn thanks to the ChromoMap R package (31).

Phasing score analyses were performed using the equation from De Paoli *et al.* (32), without strand selection, and we selected the 10-cycle window if there were more than three consecutive 21nt windows with sRNA inside.

Statistical analyses

All the statistical analyses were performed on Rstudio. Depending of samples following or not a Normal model and having homogenous variances, we performed ANOVA and *t*-Student tests with the *P*-value threshold (α) equals to 0.05, if the previous assumptions were respected, if not we performed Kruskal–Wallis and Wilcoxon tests with α equals to 0.05. When doing multiple test analysis, we corrected α by using the Holm method.

Results

The N-terminal domain of Arabidopsis AGO1 exhibits G/R-rich motifs that are symmetrically dimethylated by PRMT5 *in vivo*

In *A. thaliana*, four out of ten Argonautes proteins (AtAGO1, AtAGO2, AtAGO3 and AtAGO5) present RGG/GRG motifs, known as potential targets for PRMT5 (33) (Figure 1A). These motifs are generally clustered in the N-terminal extension (NTE) of these proteins, in a region which we will refer to as Nt-AGOs-RGG/GRG (Figure 1A–C). Among these, AtAGO2 has been already experimentally identified as a PRMT5 substrate by Hu *et al.* (21). Its closest paralog AtAGO3 stands out with an extended N-terminal region compared to all other AtAGOs and contains the most important number of predicted PRMT target sites with 26 RGG/GRG motifs (Supplementary Figure S1A). However, if we consider only the region delimited by the RGG/GRG motifs in each protein, AtAGO1 presents then the most important local density as its RGG/GRG boxes represent locally 35% of total residues (Supplementary Figure S1A).

The RGG/GRG repeats are almost exclusively located in predicted intrinsically disordered regions (IDR) that present lower sequence complexity (Supplementary Figure S1A, B). In particular, the Nt-AGO1-RGG/GRG region is clearly included in a long IDR as predicted by ANCHOR2/IUPRED3 (https://iupred3.elte.hu/), thus contrasting with the rest of the protein which is extremely structured (Figure 1B, C). Despite the lack of secondary structure conservation, the compositional bias of the Nt-AGO1-RGG/GRG region was observed in AtAGO1 orthologs from green algae (*Chlamydomonas reinnhardtii*), bryophytes (moss and liverwort), trees (*Populus trichocarpa*) and other flowering plants (Supplementary Figure S1C), supporting the idea of an ancient and conserved role assigned to these motifs.

Another interesting observation concerning AtAGO1, is that both NLS (V_2RKRR) and NES (L_{149}AQQFEQLS) motifs are present in the predicted IDR, at each side of the Nt-AGO1-RGG/GRG region (Figure 1B, C, (22)). The NLS (R_3KRR), which is conserved in terrestrial plants AGO1 orthologs (Figures 1A and S1C), is positioned almost after the initiation methionine and very close to the first predicted RGG box ($GR_{30}G$). The NLS is not conserved in AtAGO2/3/5, where it is replaced by an RGG box (Figure 1A). Together, these observations raise interesting questions regarding the potential role of the arginine/R-methylation (R-met) state in the IDR context, and more specifically its impact on AGO1 nucleocytoplasmic shuttling activity.

To address this point, we collected several *atprmt5* T-DNA insertion mutant alleles that are devoid of PRMT5 protein, sDMA deposition on proteins and exhibit the same developmental defects, including the previously reported delay in flowering (Figures 1E and S2) (34). We then immunopurified AGO1 protein from either wild type or *prmt5* mutant plants and investigated whether this protein is R-methylated by PRMT5 by performing western blot using anti-sDMA specific antibodies. These IPs were performed using buds which present two main advantages here: a high protein accumulation (tissue where AtAGO1 is the most abundant, as illustrated in Supplementary Figure S3), and a functional relevance (as AtAGO1 is known to play a crucial role in meristems and flower development; (35). As shown in figure 1D, AtAGO1 proteins purified from wild type, but not *prmt5* mutant buds,

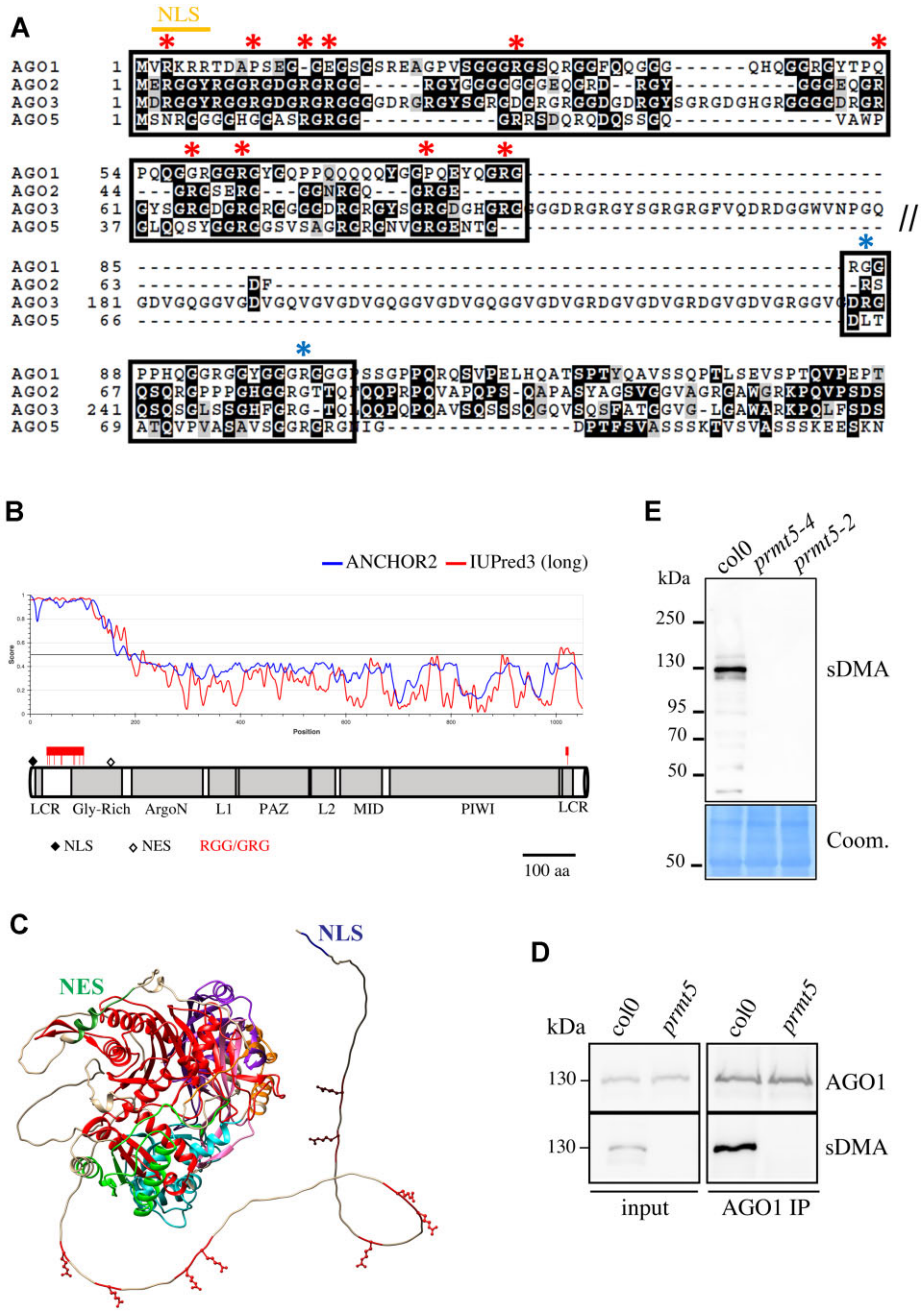

Figure 1. AGO1 protein exhibits conserved RGG/GRG motifs mainly clustered in the N-terminal disordered region in plants and is R-symmetrically methylated by PRMT5 enzyme in *A. thaliana*. (**A**) RGG/GRG boxes are present in AGO1/2/3/5 N-terminal regions in *A. thaliana*. AtAGO1/2/3/5 sequences from TAIR10 Genome (Phytozome v12.1) are aligned using clustalW and only the N-terminal residues of interest (upstream the ArgoN domain) are presented here. This analysis is extended to AGO1 protein from all green lineage available in database in Supplementary Figure S1. AtAGO1 NLS (position 2–6) is indicated respectively above AtAGO1 sequence (22). For additional info, NES is at position 149–159. The red asterisks highlight well conserved predicted methylated arginines in this alignment. The blue asterisks highlight the predicted methylated arginines which are not considered to be as well conserved in this alignment. B-C; RGG/GRG motifs are located in unstructured regions in AtAGO1. (**B**) Prediction of long intrinsically disordered regions in red (IUPred3) and protein binding regions in disordered proteins in blue for AtAGO1 (ANCHOR2) using IUPred3 tool (https://iupred.elte.hu/). A graphical representation at scale of AtAGO1 domains is presented under the predictions, with RGG/GRG boxes shown in red. (**C**) Predicted 3D structure of AtAGO1 obtained from AlphaFold protein structure database (https://alphafold.ebi.ac.uk/). The NLS signal is highlighted in dark blue, and the NES signal is highlighted in dark green. The predicted dimethylated arginines have their lateral chain shown and coloured. Finally, from the N-ter to the C-ter of the proteins, we have the ArgoN domain (in purple), the Argonaute linker 1 domain (in pink), the PAZ domain (in blue), the Argonaute linker 2 domain (in orange), the MID domain (in green), and the PIWI domain (in red). (**D**) AtAGO1 exhibits PRMT5 dependent sDMA modifications. Symmetrically dimethylated arginine modifications are identified here on inputs and AGO1 IP extracts obtained from col0 and *atprmt5-6* buds. AGO1 protein is immunoprecipitated using anti-AGO1 antibodies (Agrisera) and eluted by competition using the AGO1 peptide used as antigen for antibodies production (Eurogentec). AGO1 and sDMA modifications are detected by western blot using respectively anti-AGO1 (Agrisera) and anti-sDMA antibodies (Cell Signaling Technology, CST) visualized by chemiluminescence. (**E**) The PRMT5 enzyme catalyses all detectable sDMA modifications in *A. thaliana* buds. Total proteins (20 μg) from col0 and *atprmt5-6* (Hurkman and Tanaka protocol) (27) are used to detect HMW polypeptides harbouring symmetrically DiMethylated Arginine with anti-sDMA antibodies (CST). The membranes are afterwards stained with colloidal coomassie after immunodetection to provide loading controls.

exhibits sDMA marks, thus confirming that AtAGO1 is a target of PRMT5 *in planta* (Figures 1D). Moreover, we noticed that the 130kDa AtAGO1 protein corresponds to the predominant sDMA-modified target in whole protein extract (Figures 1D, E and S4B), highlighting AGO1 as a major target of PRMT5 *in vivo*.

AtAGO1 is also targeted by another type I PRMT *in vivo*

To further identify the arginine/R residues that are modified by PRMT5, we assessed the post-translational modification signatures of purified AGO1 by nano LC–MS/MS. These experiments have been performed with buds of wild type plants and two independent *prmt5* knockout mutants. The R residues identified as preferentially dimethylated (DiMethyl/R or DiMeR) in the Nt-AGO1-RGG/GRG region of wild type AGO1 are summarized in figure 2A (list of spectra in Supplementary Table S1), and correspond mostly to R_{30}, R_{34} and R_{101}. The dimethylation state of R residues in the other RGG/GRR motifs (R_{48}, R_{59}, R_{62}, R_{83}, R_{85}, R_{94}) cannot be accurately assessed probably due to the lack of peptides spanning the region in the nano LC-MS/MS analysis (Supplementary Figure S4C). Unexpectedly, we have underscored that AtAGO1 protein still contains dimethyl/R modifications at most RGG/GRG positions in both *atprmt5* mutant backgrounds, a result that seems to contradict our earlier anti-sDMA western assays. As the LC–MS/MS procedure does not allow to discriminate between sDMA and aDMA, we have next addressed the possibility that the RGG/GRR motifs may be ectopically modified by a type I PRMT in the absence of PRMT5 enzyme. To answer this question, we have immunopurified AtAGO1 from both wild type and *atprmt5* mutant and detected the aDMA marks using specific antibodies. This analysis indicated that AtAGO1 is solely modified with aDMA marks in *prmt5* background (Figures 2B and S4A). In contrast, both sDMA and aDMA marks are observed in AtAGO1purified from wild type plants, indicating that AtAGO1 can be targeted by both PRMT-types enzymes in native plants. To confirm this observation in a more controlled manner, we have introduced *atprmt5* mutation into a *pAGO1-GFP-AGO1/ago1-3* line that expresses a fluorescent and functional version of AtAGO1 (22). The F3 progenies *pAGO1-GFP-AGO1/ago1-3/prmt5* exhibit the same developmental defects as the parent *prmt5* single mutant (Figure 2C), i.e. delay in flowering, defects in SAM maintenance, greener and downward curled leaves, altered fertility … (34,36,37). In line with our previous observations on endogenous AGO1, the immunoprecipitated GFP-AGO1 protein is specifically R-methylated by PRMT5 as determined by western blot with anti-sDMA antibodies, and also by another type I PRMT as depicted with by anti-aDMA signal in the reference complemented line and in the *prmt5* background (Figure 2D and S4D), lending further support to the assumption that AtAGO1 is a dually targeted by two types of PRMTs *in planta*.

AtAGO1 interacts with TSN proteins, and this association is favoured by the presence of sDMA modifications

So far, the Tudor domain is the primary reader identified to bind sDMA motifs in eukaryotes (38–40), and the roles of Tudor domain containing proteins in germline development and fertility have been well described in metazoan (41–43). Actually, many evidences support that extended Tudor domains (eTudor)-containing proteins (44,45) such as TSN (Tudor Staphyloccocal Nuclease) are *bona fide* AGO/PIWI sDMA readers, as has been shown more recently for plants (18-21,46). Arabidopsis encodes two TSN proteins, AtTSN1 and AtTSN2, which are highly similar (84% of identity) and functionally redundant (47). To assess if AtTSN proteins also recognize the sDMA modifications of AtAGO1, we have performed independent AGO1 co-IPs experiments using buds or flowers total protein extracts from a wild type or two independent *atprmt5* mutant lines (Figure 3, Supplementary Table S1). As both AtTSN and the AGO1-interacting protein SDE3 (SILENCING DEFECTIVE3) migrate at the same size as AtAGO1 in standards SDS-PAGE gels (Supplementary Figure S5A for AtTSN detection; 49), we used gel slices centred around the immunoprecipitated AtAGO1 protein to perform nano LC-MS/MS analyses for each co-IP, and to finally quantify the impact of sDMA loss on its association with AtTSN and SDE3 proteins (Figure 3A). Knowing that SDE3 binds AtAGO1 through WG/GW-type AGO hook motifs that act through a mechanism distinct from R-methylation (48,49), we infer that the number of SDE3 peptides recovered in each IP would be a good proxy of the AGO1 co-IP efficiency. Both the Coomassie-stained gels and the total number of peptides identified for AtAGO1 using two spectral count quantification methods relying either on Mascot algorithm or Sequest algorithm (Proteome Discoverer software package, Thermo) show that all these AGO1-IPs are highly consistent (Figures 3A, B, Supplementary Table S1, Supplementary Figure S6A). The mascot score thresholds obtained are almost the same for all analysed samples, supporting also the quality of these experiments (table in Figure 3A). As expected, a very similar number of SDE3 peptides was recovered confirming the comparative efficiency of the three AGO1-IP experiments (Figure 3C, Supplementary Figure S6A). In contrast, the number of AtTSN1/AtTSN2 peptides recovered from MS analysis was specifically decreased in all *prmt5* samples analysed (Figure 3C, Supplementary Figure S6A), a reduction that is not due to an overall reduction of TSN-type protein levels in the *atprmt5* backgrounds (Supplementary Figure S5B). To reinforce our conclusions, we have applied the gold-standard MS quantification method called MS1 label-free quantification or EIC (Extracted Ion Chromatogram). It relies on the reconstitution of the elution peaks of the three best TSN1 and TSN2 peptides and the comparison of the intensities of these elution peaks in Col-0 and *prmt5* mutants (Figure 3D; S6B, C and Supplementary Table S1 sheet EIC). Figure 3D shows the elution peaks from one specific TSN1 peptide and one specific TSN2 peptide. These analyses confirm that TSN proteins are less abundant but still detectable in AGO1 IP from *prmt5* mutants. The AGO1/TSN association was also assessed by GFP IPs using the GFP-AGO1 transgenic lines followed by western blot. Supplementary Figure S6D shows that this association is not completely abolished when PRMT5 is not present. Taken together, these observations suggest that AtAGO1 does indeed associate with AtTSNs *in vivo*, and that this association is favoured by the sDMA modifications.

AtAGO1 trafficking in the cell is not affected in *prmt5* mutants

It has been proposed that the activity of AGO1 in Arabidopsis requires its nucleo-cytosolic trafficking, and that the

A

Sample	Col0	*prmt5-2*	*prmt5-4*
Total number of spectra (AGO1)	1757	1660	2287
Sequence coverage AGO1 (%)	66%	68%	68%
Normalization Factor	1,30	1,38	1,00
Mascot threshold (p<0.05)	32	32	33

Sample	Col0			*prmt5-2*			*prmt5-4*	
Residue position	Maximal Mascot score	Total number of spectra	Normalized number of spectra	Maximal Mascot score	Total number of spectra	Normalized number of spectra	Maximal Mascot score	Normalized number of spectra
DiMethyl(R30)	39	9	11,70	41	10	13,8	37	5
DiMethyl(R34)	23	2	2,60	61	11	15,18	53	22
DiMethyl(R59)				29	3	4,14	26	8
DiMethyl(R62)				97	13	17,94	93	20
DiMethyl(R83)				28	2	2,76	21	2
DiMethyl(R85)				28	2	2,76	27	4
DiMethyl(R94)				18	1	1,38	24	2
DiMethyl(R101)	34	10	13,00	46	11	15,18	45	15

Maximal Mascot score: p<0.05, p>0.05

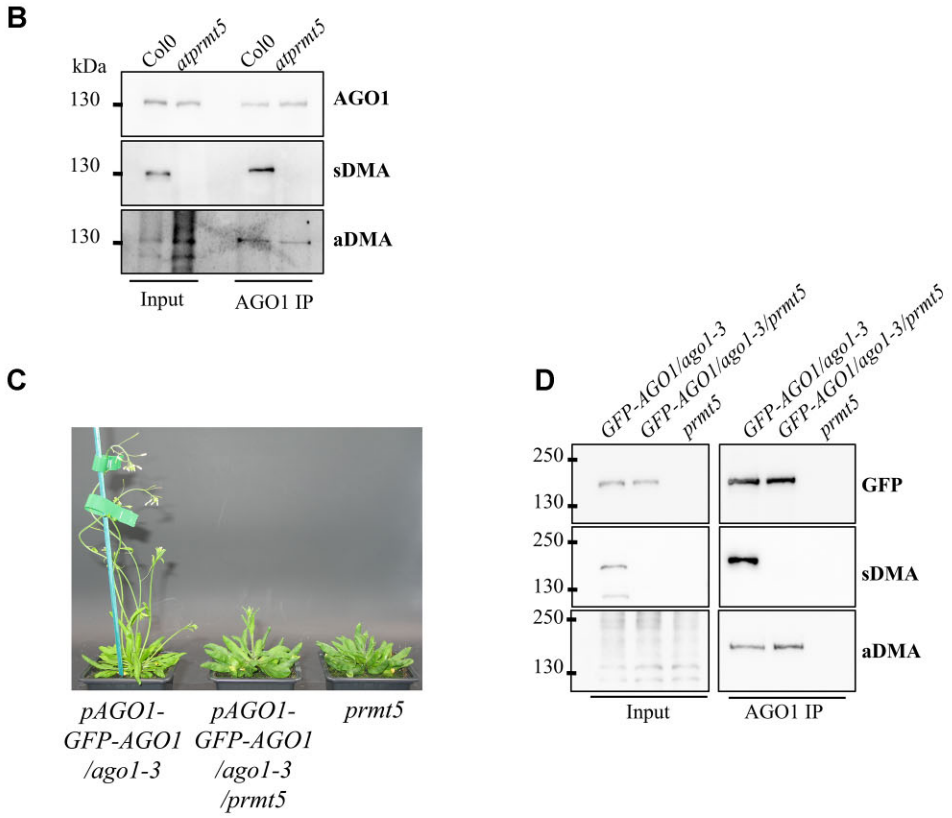

Figure 2. the Nt-AGO1-RGG/GRG domain contains dual dimethyl/R marks in *A. thaliana*. (**A**) The Nt-AGO1-RGG/GRG region still harbours dimethyl/R modifications in *atprmt5* mutants. AtAGO1 IPs are performed from wild type, *atprmt5-2* or *atprmt5-4* buds using the anti-AtAGO1 antibodies. Immunoprecipitated proteins are separated by SDS-PAGE and the gel is then stained with colloidal coomassie. A band around 130 kDa is excised for each IP for further nanoLC–MS/MS analyses (QExactive + Orbitrap Mass Spectrometer, ThermoFisher Scientific) to identify of dimethyl/R marks present on AtAGO1. The total number of spectra matching on AtAGO1 was used to normalize the 3 samples Col0, *atprmt5-2* and *atprmt5-4* (normalization factor). The modification DiMethyl/R was set as variable during the Mascot database search. Eight arginine residues were identified as dimethylated: the total number of spectra matching to each modified arginine was computed and then normalized by the total number of AtAGO1 spectra. Spectra matching on AtAGO1 sequence were finally validated respecting the Mascot identity threshold ($P < 0.05$) by comparing the maximal Mascot score for the set of spectra matching on a dimethylated residue to the Mascot identity threshold (green if $P < 0.05$, red if $P > 0.05$). (**B**) AtAGO1 harbours asymmetrically DiMethyl arginine (aDMA). Asymmetrically dimethylated arginine modifications are identified here on inputs and AtAGO1 IP extracts obtained from col0 and *atprmt5-6* buds. AtAGO1 protein is immunoprecipitated using anti-AtAGO1 antibodies (Agrisera) and eluted by competition using the AtAGO1 peptide used as antigen for antibodies production (Eurogentec). AtAGO1 protein is detected by western blot using anti-AGO1 (Agrisera) and both R/dimethyl marks are specifically detected using either the anti-sDMA (CST) or anti-aDMA antibodies (CST). Immunodetection is visualized here by chemiluminescence. (**C**, **D**) The GFP-AtAGO1 protein recapitulates the R-met pattern of an endogenous AtAGO1. C; Presentation of *pAtAGO1-AtAGO1-GFP/ago1-3/atprmt5* triple mutant; (C) *pAtAGO1-AtAGO1-GFP/ago1-3* line has been introgressed in *atprmt5-4* mutant. Photographs of triple homozygous F3 progeny and parental lines are presented (38-day-old plants, cultivated in long-day period, with Vegeled LED lights). (D) The GFP tagged version of AtAGO1 loses sDMA modifications, and still contains aDMA marks in the absence of AtPRMT5 enzyme. GFP-AGO1 is immunoprecipitated using anti-GFP nanotrap magnetic beads (proteintech). GFP-AGO1 and sDMA modifications are identified in inputs and IP products by western blot. Chemiluminescence was used to detect respectively anti-GFP (JL-8 antibody, Clonetech/Takara) and anti-sDMA antibodies.

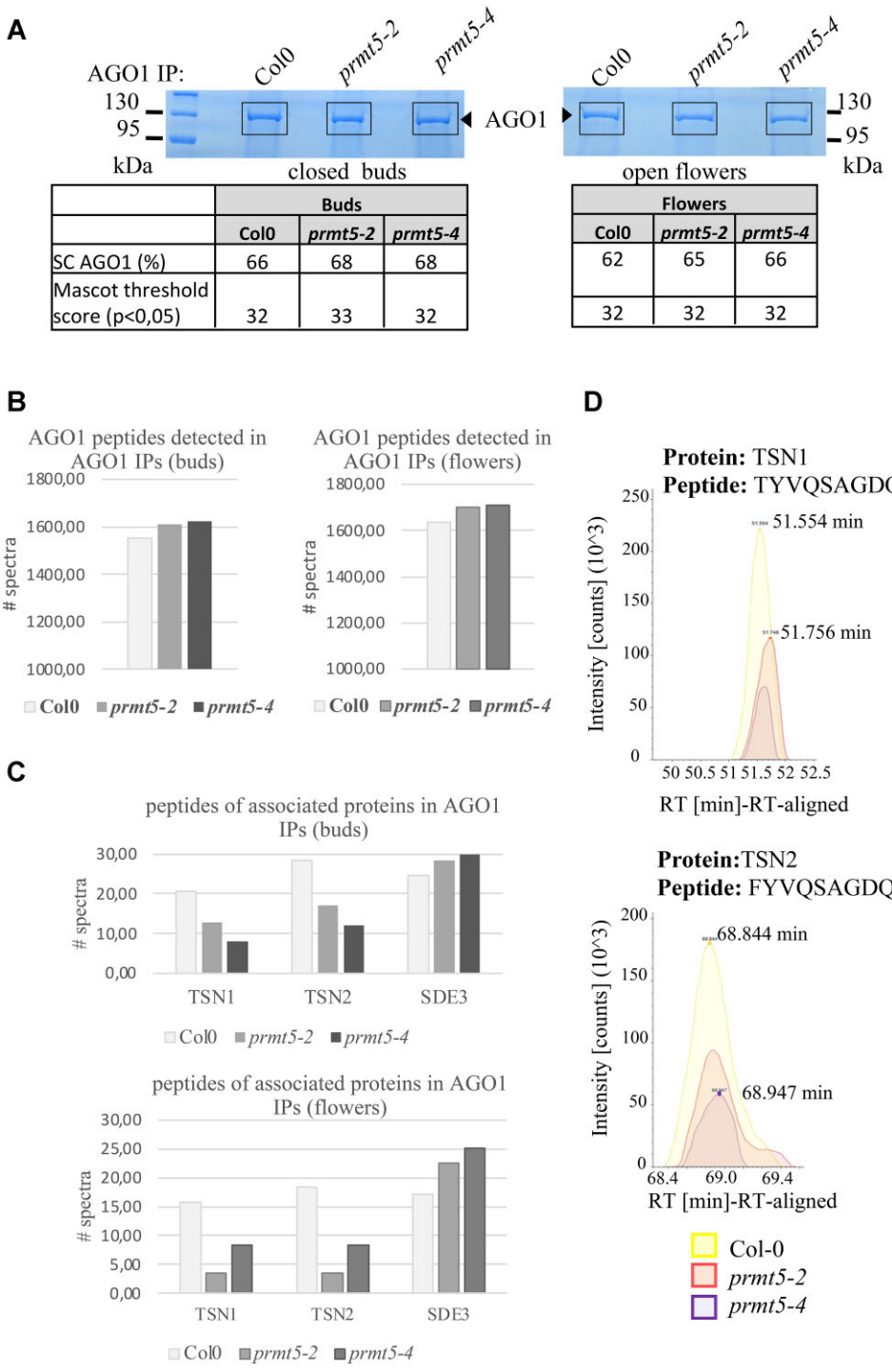

	Buds		
	Col0	*prmt5-2*	*prmt5-4*
SC AGO1 (%)	66	68	68
Mascot threshold score (p<0,05)	32	33	32

Flowers		
Col0	*prmt5-2*	*prmt5-4*
62	65	66
32	32	32

Figure 3. sDMA modifications of AtAGO1 favour AGO1/TSN interaction *in vivo*. **A**) Internal controls for LC–MS/MS analyses from AtAGO1 IPs performed in wild type and in both *atprmt5-2* and *atprmt5-4* mutants. AtAGO1 IPs are performed from buds (left) and opened flowers (right) extracts using the anti-AtAGO1 antibodies. We precise that the buds experiments analysed here are the same used for Figure 2A. Immunoprecipitated proteins are separated by SDS-PAGE and the gel is then stained with colloidal coomassie (upper part). A band around 130 kDa (framed in the gels) is excised for each IP for further nanoLC-MS/MS analyses (QExactive + Orbitrap Mass Spectrometer, ThermoFisher Scientific). Only proteins identified in the TAIRv10 database and presenting a Mascot pretty rank equal to 1, PSM (Peptide Spectrum Match) score above 25, and 1% FDR (False Discovery Rate) on both PSM and protein sets (based on score) are validated. The AtAGO1 sequence coverage (%) and the mascot threshold scores with a *P*-value <0.05 are presented as a table below. (**B**, **C**) AtTSN proteins interact preferentially with a symmetrically dimethylated AtAGO1 form. The total spectra number of peptides identified in AtAGO1 IPs from buds (left) and flowers (right) presented as histograms, (B) for AtAGO1, (C) for AtTSN and AtSDE3. The spectral counts associated to the bait AtAGO1 and its partners are also recapitulated in the table 1 according to corresponding basic or specific spectral counts (Mascot algorithm). (**D**) Reconstitution of the elution peak area for the best identified peptide of TSN1 protein, used for an additional Label-free (MS1) quantification method (see Supplementary Table S1, sheet EIC). The elution peak is extracted from ion chromatograms obtained during LC–MS/MS and represented by the intensity of counts according to the relative retention time (RT, in minutes) for each peptide.

protein shuttling is controlled by two NLS and NES motifs that are located in the N-ter region (Figure 1A–C) (22). The proximity of these motifs with the Nt-AGO1-RGG/GRG-methylated region raises questions concerning the potential impact of the observed PRMT5-dependent R-met on the trafficking and subcellular localization of AtAGO1 *in vivo*. To address this point, confocal microscopy observations in roots of 7-day-old *pAGO1-GFP-AGO1/ago1-3/prmt5* seedlings however reveal that the cytosolic steady state localization of GFP-AGO1 is not modified in the absence of PRMT5 compared to the reference *pAGO1-GFP-AGO1/ago1-3* line (Figure 4A). We then challenged the nucleo-cytosolic shuttling activity of GFP-AGO1 in these two lines by adding Leptomycin B, a well-known and specific nuclear export inhibitor. Leptomycin B treatment leads to nuclear retention of GFP-AGO1 of both *pAGO1-GFP-AGO1/ago1-3* and *pAGO1-GFP-AGO1/ago1-3/prmt5* roots, suggesting that NLS, and the NES, remain accessible and functional when AtAGO1 is not symmetrically dimethylated (Figure 4A). We can then conclude that PRMT5 dependent regulation is not involved in AGO1 nucleocytoplasmic trafficking.

The action of Tudor containing proteins, and more interestingly the Tudor-sDMA module, is associated to nuclear or cytoplasmic mRNP condensates or foci dependent activities (50–53). Besides, R-met of some proteins has also been shown to drive phase separation in human cells (54). Concordantly, the two Arabidopsis TSN proteins are mainly involved in plant tolerance to abiotic stresses (47). They also play a role in the assembly and the communication between two distinct cytoplasmic mRNP entities, the constitutive processing-bodies (P-bodies) and the stress granules (SG) induced specifically upon stress (55,56). To investigate the role of sDMA in AtAGO1 dynamic in response to an abiotic stress, we have selected HS conditions that trigger the formation of stress granules in reporter lines (as depicted by the RFP-PAB2 cytosolic foci in Supplementary Figure S7). In parallel, we have also checked that *prmt5* mutation, and so the loss of all sDMA modifications in cell, do not compromise to the assembly of stress granules and p-bodies distribution in *A. thaliana* (Supplementary Figure S7). Then, we have used our previously established *pAGO1-GFP-AGO1/ago1-3* plants to monitor AGO1 distribution in the same conditions. At standard temperature (20°C), AtAGO1 is evenly distributed in the cytosol of root tips cells of 5-day-old seedlings. Remarkably, when we apply the HS, AtAGO1 is partly and specifically relocated into heterogeneous cytosolic foci (Figure 4B). The same profile is observed upon HS when GFP-AGO1 is expressed in the *prmt5* background, emphasizing that globally, AtAGO1 dynamic is not significantly modified in *prmt5* mutants.

The landscape of miRNAs loaded into AtAGO1 is not drastically affected in the absence of PRMT5

Our evidence that AtAGO1 is a target of PRMT5, prompted us to address the contribution of the sDMA modifications in the control of AGO1 activity and regulation *in planta*. As a first step, we have assessed the accumulation of AGO1 level in different tissues of both wild-type and *prmt5* mutant backgrounds. Western blot analyses indicated that the *atprmt5* mutation has barely no impact on the accumulation of AtAGO1 in total extracts from the reproductive organs, young seedlings and roots (Figure 5A and S8) (27), or native and soluble proteins from buds, which globally correspond here to the input fractions used for IPs (Figures 1D and 2B). Likewise, the accumulation of AtAGO1 was not affected in the *attsn1,attsn2* double mutant background reinforcing the idea that the sDMA modifications have little impact on AtAGO1 accumulation (Supplementary Figure S5C). We next addressed the role of PRMT5 and associated sDMA marks in the activity of AtAGO1 effector by introgressing two *prmt5* mutations in the *pSUC-amiRSUL* sensor line, which reports AGO1-dependent miRNA activity *in vivo* (25). The *pSUC-amiRSUL* construct leads to the production in the phloem companion cells of an artificial miRNA designed to target the *SUL/CHLI-1* transcript encoding a protein involved in chlorophyll biosynthesis, and thereby triggering a vein-centred chlorosis. Therefore, the defects in miRNA dependent pathway can be phenotypically monitored. The *pSUC-amiRSUL/prmt5* plants do not exhibit a clear impact of the chlorotic phenotype, as confirmed by the integrated chlorosis density (Figure 5B and S9A). Furthermore, complementary molecular analyses do not highlight any significant change in *SUL* transcript and SUL protein levels in *pSUC-amiRSUL/prmt5* plants compared to *amiRSUL* parental line (Figures 5C, D; S9B, C). To conclude, the results obtained with this sensor line does not support a role for sDMA modifications in AtAGO1 miRNA dependent action.

Then, to go further, we have assessed the miRNA loading capacity of AtAGO1 in the absence of PRMT5 enzyme. For this purpose, biological duplicates have been generated from buds, and each biological replicate includes one wt and two distinct *atprmt5* mutants (Supplementary Figure S10A). The miRNAs sequenced have been identified using miRbase v22.1 (https://www.mirbase.org/) and classified according to their size (21- to 24nt-long) (Supplementary Table S2, sheet3). We first considered the miRNA landscape in total extracts (inputs used for AtAGO1 IPs) for each *atprmt5* mutant compared to wt. We have observed that the accumulation of 22-nt long miRNAs is not impacted, while among all 21 nt long-miRNAs, only four can be considered here as more present in both *atprmt5* mutants (Supplementary Figure S10B for 21/22nt-long miRNAs; Supplementary Table S2). So, this analysis shows that the steady states level of almost all miRNAs are not affected when PRMT5 is not expressed. Next, we have analysed the set of AtAGO1 Differentially Loaded miRNA (DL-miR) in *atprmt5* using AGO1-IPs (from the same inputs previously described). We have looked at miRNAs that can be differentially detected in AGO1 IPs for each *atprmt5* mutant compared to wt (Figure 5E, Supplementary Table S2). With the exception of ath-miR156b-3p, neither 23- nor 24-nt-long miRNAs differ significantly (Supplementary Table S2). So, we have focused the following analyses on 21 and 22 nt-long miRNAs. To establish the Differentially Loaded miRNA (DL-miR) sets of 21- and 22- nt long miRNAs, we have compared the miRNAs in AtAGO1 IPs for each *atprmt5* mutant compared to wt in each replicate, to ultimately select only miRNAs that are consistently standing out on both biological replicates (Supplementary Table S2, sheet 8). This work is represented as a boxplot in Figure 5E, and highlights that very few 21/22 nt-long miRNAs can indeed be considered as DL-miRNA (only 10 DL-miR identified and listed in Supplementary Table S2 among the 430 mature miRNA referenced in miRbase). Among those, we do not observe any bias for up- or down-regulated association in AtAGO1. Therefore, these results suggest that the landscape of miRNA loaded into AtAGO1 is not drastically affected in the absence of PRMT5.

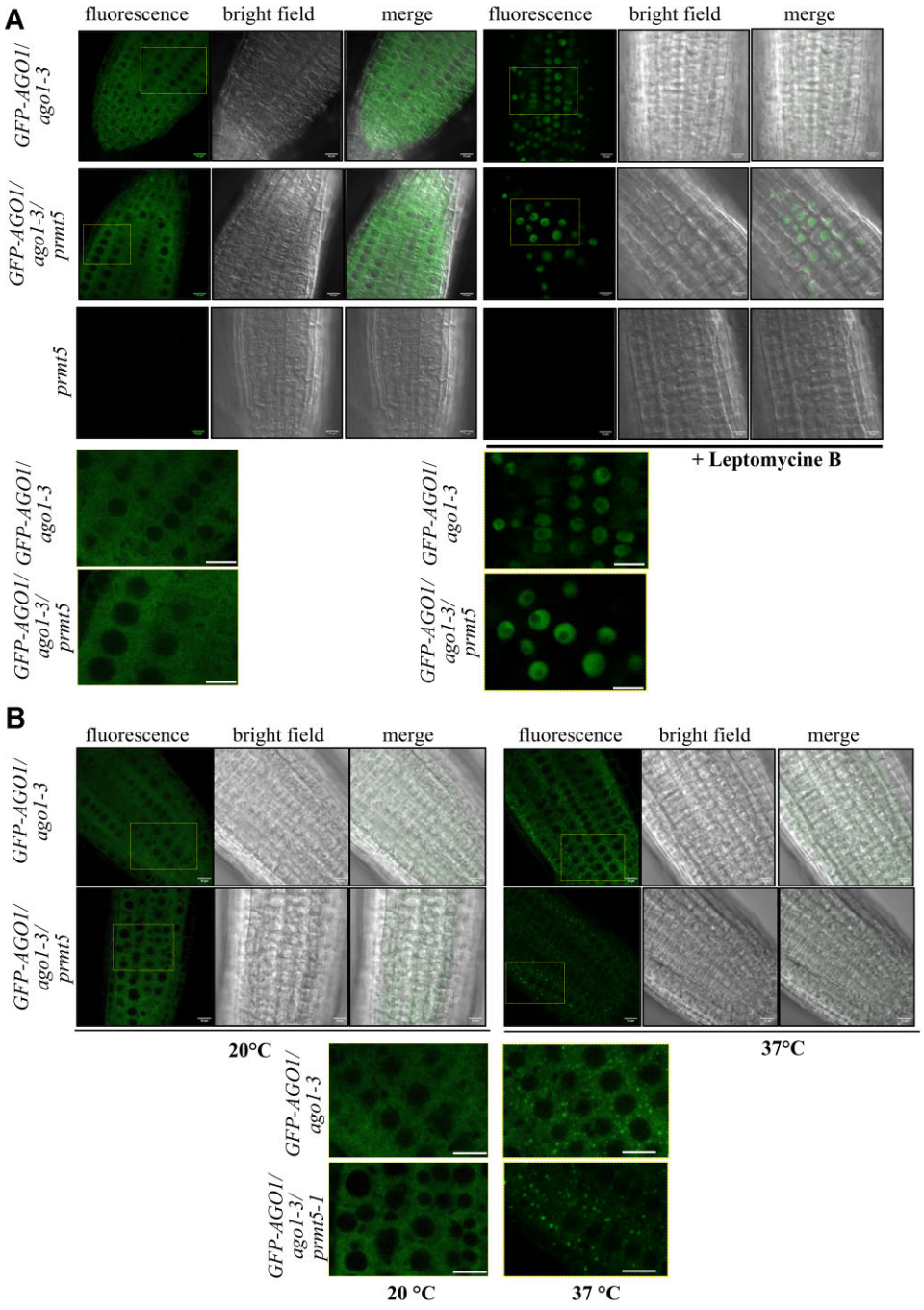

Figure 4. The loss of sDMA modifications do not abolish AGO1 trafficking in the cell. (**A**) AtAGO1 protein can still shuttle between cytosol and nucleus in the *atprmt5* mutant. Localisation of AtAGO1 in root apex of 7-day-old seedlings grown in standard conditions. The seedlings have been exposed or not to leptomycin B treatment prior to confocal microscope acquisitions. Yellow dotted frames depicted in the GFP acquisition images are scaled up below. Same conclusion obtained with *pAGO1-AGO1-GFP/ago1-3/prmt5-6* seedlings (not shown). Scale bar, 10 μm. (**B**) AtAGO1 relocalizes in cytoplasmic foci upon heat stress and this response is not dependent of its sDMA status. General overview of root apex of 5-day-old seedlings expressing a GFP-tagged AGO1 in *ago1-3* or in *ago1-3/prmt5-4* backgrounds. The GFP-AGO1 construct is controlled by AtAGO1 endogenous promoter (Bologna *et al.*, 2018). Images obtained by confocal microscopy. Yellow dotted frames depicted in the GFP signal images correspond to the selected zone scaled up below. Same conclusion obtained with *pAGO1-AGO1-GFP/ago1-3/prmt5-2* seedlings. Scale bar, 10 μm.

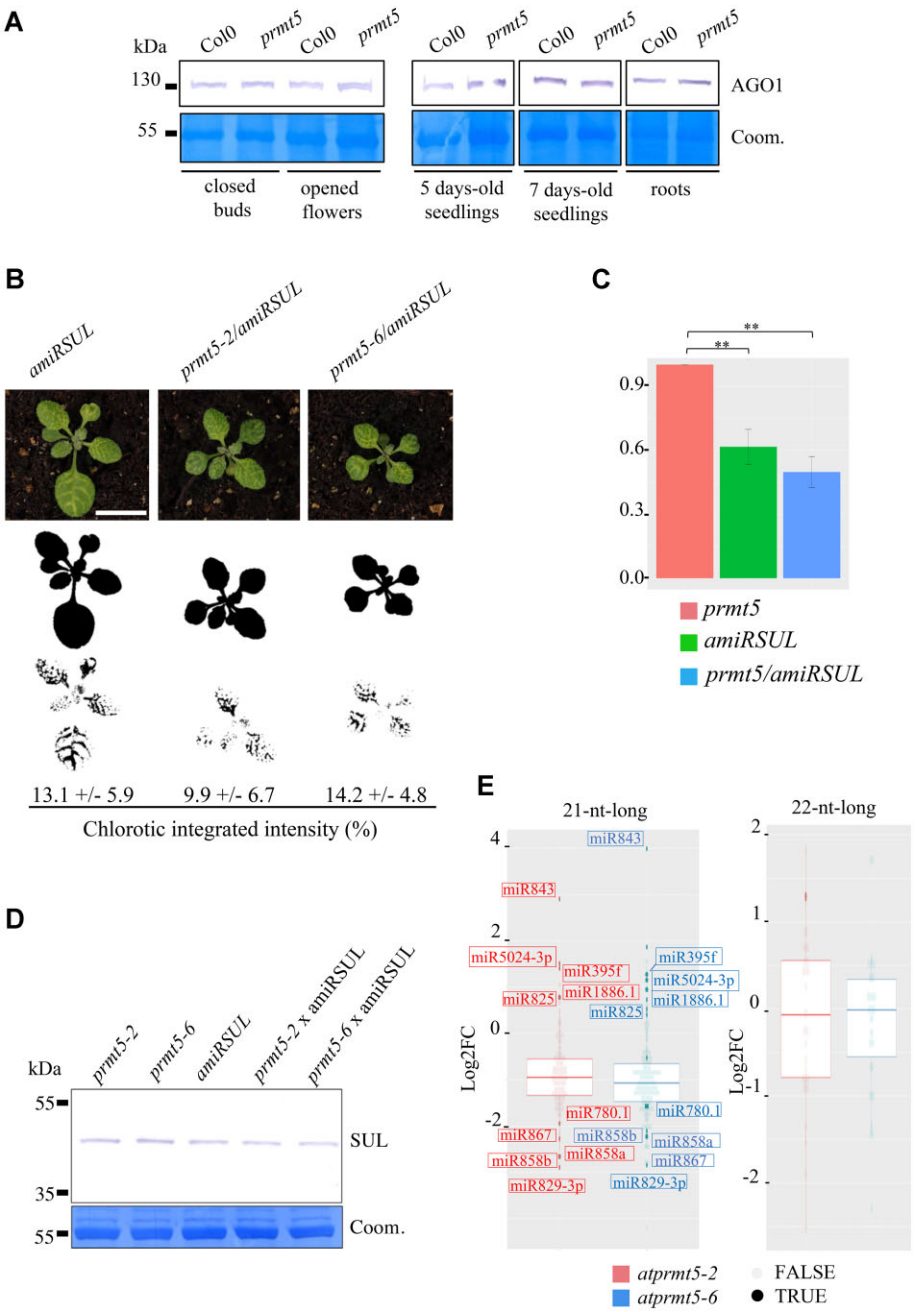

Figure 5. The *atprmt5* mutation does not impact AtAGO1 accumulation and miRNA loading in *Arabidopsis thaliana*. (**A**) AtAGO1 level is not regulated by PRMT5 in all stages and tissues used in this study. AtAGO1 is detected in total protein extracts from col0 and *atprmt5-4* buds, flowers, roots, and 5/7/21-day-old seedlings. After separation by SDS-PAGE and protein transfer, AtAGO1 immunodetection is performed using anti-AGO1 antibodies and visualized directly on membrane by colorimetric method. The membranes are then stained with colloidal Coomassie as loading controls. This figure is selected and representative of two biological replicates. (B–D) amiRSUL directed RNA silencing is still effective when sDMA modifications are abrogated. (B) Analyses of *atprmt5/amiRSUL* leaves. Photographs of whole plants from *amiRSUL*, *atprmt5-2/amiRSUL* (F4), *atprmt5-6/amiRSUL* (F4) 18-day-old seedlings. These photographs are converted into binary images to get the corresponding seedling surface area and chlorotic phenotype panels. Finally, quantitative analyses were performed using ImageJ 1.53k to define the chlorotic integrated density (estimated in %). Scale bar 1 cm. (**C**) Analyses by RT-qPCR of *SUL* transcripts levels in the total aerial parts of seedlings from *atprmt5/amiRSUL* (F4) and *atprmt5, amiRSUL* parental lines. *ACTIN7* is used as internal control and the *atprmt5* samples selected here as the reference level for *prmt5/amiRSUL* while Col0 samples are used as the reference level for *amiRSUL*. The histogram shown here is obtained by four biological replicates which include two independent lines for *prmt5*, and *prmt5/amiRSUL*. These both independent lines are pooled for each genotype to perform statistical analyses, and only results considered as significantly different are depicted ('**' for *P*-value < 0.01 using Wilcoxon test corrected with Holm, *P*-value < 0.05). (**D**) SUL protein level is assessed by western blotting performed on 5 micrograms of total proteins of seedlings aerial parts from *atprmt5-2/amiRSUL* (F4), *atprmt5-6/amiRSUL* (F4) and *atprmt5-2*, *atprmt5-6*, *amiRSUL*, parental lines. SUL protein detection is achieved with anti-SUL/CHL-42/CHL-I polyclonal antibodies (73) and revealed by colorimetric method. The membrane is then stained with colloidal Coomassie to provide internal loading control E; miRNA loading into AtAGO1 is barely not affected in reproductive tissues of *atprmt5* mutants. Boxplot analyses of miRNAs Differentially Loaded (mi-DL) into AtAGO1 in buds from *atprmt5-2* and *atprmt5-6* compared to wild type. Coloured and non-transparent points (red for *atprmt5-2*/wt and blue for *atprmt5-6*/wt) highlight significant mi-DL with *P*-values < 0.05 and only mi-DL identified in both mutants are framed and annotated. The top panel corresponds to 21-nt-long miRNA, while the bottom panel corresponds to 22-nt-long miRNA.

A panel of phasiRNA is less loaded when AGO1 is not symmetrically R-methylated

Defects in siRNA and piRNA loading have been previously described respectively for AtAGO2 and others metazoan AGO proteins in *prmt5*-type mutant backgrounds (18,19,21). These observations led us to further investigate the loading status of siRNAs in AGO1 in the *atprmt5* mutants in order to identify AGO1 Differentially Loaded 21nt-long siRNA (DL-siRNA) in *A. thaliana* buds. We used the same datasets as described above for the analyses of AtAGO1-miRNAs association (Supplementary Figure S10A, Supplementary Table S2). We have first examined the overall distribution of loaded sRNAs and conclude that the *prmt5* mutations in Arabidopsis do not alter either AGO1's preference for 21 nt-long RNAs or the 5′U bias observed at their terminal position (Supplementary Figure S10C, D). Next, siRNA detected in inputs and AGO1 IPs are then mapped to TAIR10 genome using sliding and non-overlapping 100 bp windows and DEseq analyses are performed (Supplementary Table S2, sheet 9). Then, we have identified DL-siRNAs by using each *atprmt5* mutant compared to col0 (Supplementary Table S2, sheet 10) and plotted them in a chromomap figure in order to visualize the location of triggering loci. Figure 6A includes also a heatmap scale onto chromosomes to link these positions to observed variations. Intriguingly, this genome-wide view shows clear distinct patterns in both *atprmt5* mutants compared to wild type. Indeed, we have noticed in *atprmt5* that, the loci which produce DL-sRNA preferentially associated to AtAGO1 are mainly concentrated in the centromeric and peri-centromeric regions, whereas the loci triggering DL-siRNA that tend to be less loaded in AtAGO1 are rather located in the chromosome arms. Although this differential pattern is interesting, we have decided to focus our study solely on DL-siRNAs generated from the chromosome arms as it may be more relevant for assessing the potential impact on gene expression, plant development or plant response to environment.

We then have highlighted this sub-group in the volcano plots representing the 100 bp genomic regions containing siRNA according to their statistical p-values and their relative abundance between each *prmt5* mutant and wild-type (Figure 6B and Supplementary Figure S10E). Among the siRNA down-loaded in AGO1 in *atprmt5*, a significant subset coloured in the volcano plots corresponds to phased-type siRNAs (phasiRNAs) which exhibit a 5′U preference in their 5′ terminal position (Supplementary Figure S11A, B). We can find tasiRNAs produced from *TAS1* and *TAS3* non-coding loci coloured in yellow, phasiRNAs produced from loci that have been previously identified in the work of Vargas-Asencio and Perry in 2020 (57) coloured in pink and siRNA produced from RDR6 dependent targets coloured in green (58) (Supplementary Figure S10E). Supporting the hypothesis of a defect in AGO1 loading for the corresponding siRNAs in *atprmt5* mutants, their levels are barely affected in the input fractions (Figures 6B and S10E, right panels). As expected, the accumulation of *TAS1c* and *TAS3* precursor transcripts is not significantly modified in the absence of PRMT5, as assessed by RT-qPCR (Supplementary Figure S11C). Likewise, the loading of miR173 and miR390 that guide respectively *TAS1* and *TAS3A/B* primary cleavage is unchanged in *atprmt5* compared to wild type (Figure 5E, Supplementary Figure S10E, Supplementary Table S2). To check whether these DL-siRNAs are still produced in phase, we assessed their phasing score as described in Paoli *et al.* (32). To do that, we have used data from AGO1 IP libraries as they are enriched in 21 nt-long siRNA, providing here more reads and robustness for this calculation method. This analysis is performed for representative loci for each category (*TAS* loci, RDR6-dependent loci, and others *PHAS* loci solely identified in Vargas-Asencio study in 2020; (57) and shows that the DL-siRNA are still produced in phase in the *atprmt5* mutants, suggesting that the phasing process is not abolished in *atprmt5* mutants (Supplementary Figure S11D).

Taken together, these observations converge rather to a defect in the loading state of AGO1 for a subset of phasiRNA in the absence of PRMT5 enzyme.

Discussion

AGO1 protein is modified *in vivo* by two types of PRMT enzymes in *A. thaliana*

The N-terminal extensions (NTE) of AGO proteins have been recently analysed in several works (17,21,22,24) highlighting the main interest on understanding the role of this poorly described region in AGO activity. Our study launches the question of the regulation of AGO1 protein in *A. thaliana* with a particular emphasis on the role of its NTE, which contains predicted Glycine-Arginine Rich (RGG/GRG) recognition sites for PRMT5 enzyme. We have highlighted that these motifs are largely conserved in plant AGO1 proteins, in which they are mainly organized as clusters. We have proved experimentally that AtAGO1 is symmetrically and asymmetrically dimethylated on R/arginine residues by the type II PRMT5 and some as yet uncharacterized type I PRMTs, respectively. To date, this dual regulation has only been identified for very few proteins: the master transcription factor E2F-1 known to regulate growth, cell cycle and apoptosis; $CFLAR_L$, an anti-apopotic protein, and the histone H3 in metazoans and the histone H4 both in animals and plants (59,60). Interestingly, we have shown that both sDMA and aDMA marks can target the same RGG/GRG motifs and that in absence of PRMT5, the aDMA mark is still present in the Nt-AGO1-RGG/GRG region. This is quite exceptional as the targeting of the same R residues by type I and type II PRMTs has been so far only described for histone residues H3R2 and H4R3, the latter being the only known example in plants (61–63). It has been proposed that the nature of dimethyl/R modifications can influence protein-protein or DNA/RNA-protein interactions, and lead to either redundant or to antagonistic effects as illustrated by H4R3 regulation (34,64). Our observations also raise the question of a potential competition or hierarchy between both types of PRMTs for substrate recognition and access to the Nt-AGO1-RGG/GRG region (65). This may be of particular interest for AGO1 activity fine tuning during specific developmental stages or in response to environment. The identification of the enzyme that deposits aDMA marks on AtAGO1 among the seven type-I AtPRMT will help to understand the crosstalk between Dimethyl/R methylations and the relevance of this functional interplay in AtAGO1 functions.

AtAGO1 interacts with AtTSN proteins, but this association is not exclusively sDMA dependent

In germlines of metazoan, the recognition of sDMA marks on AGO/PIWI by Tudor domain-containing proteins drives

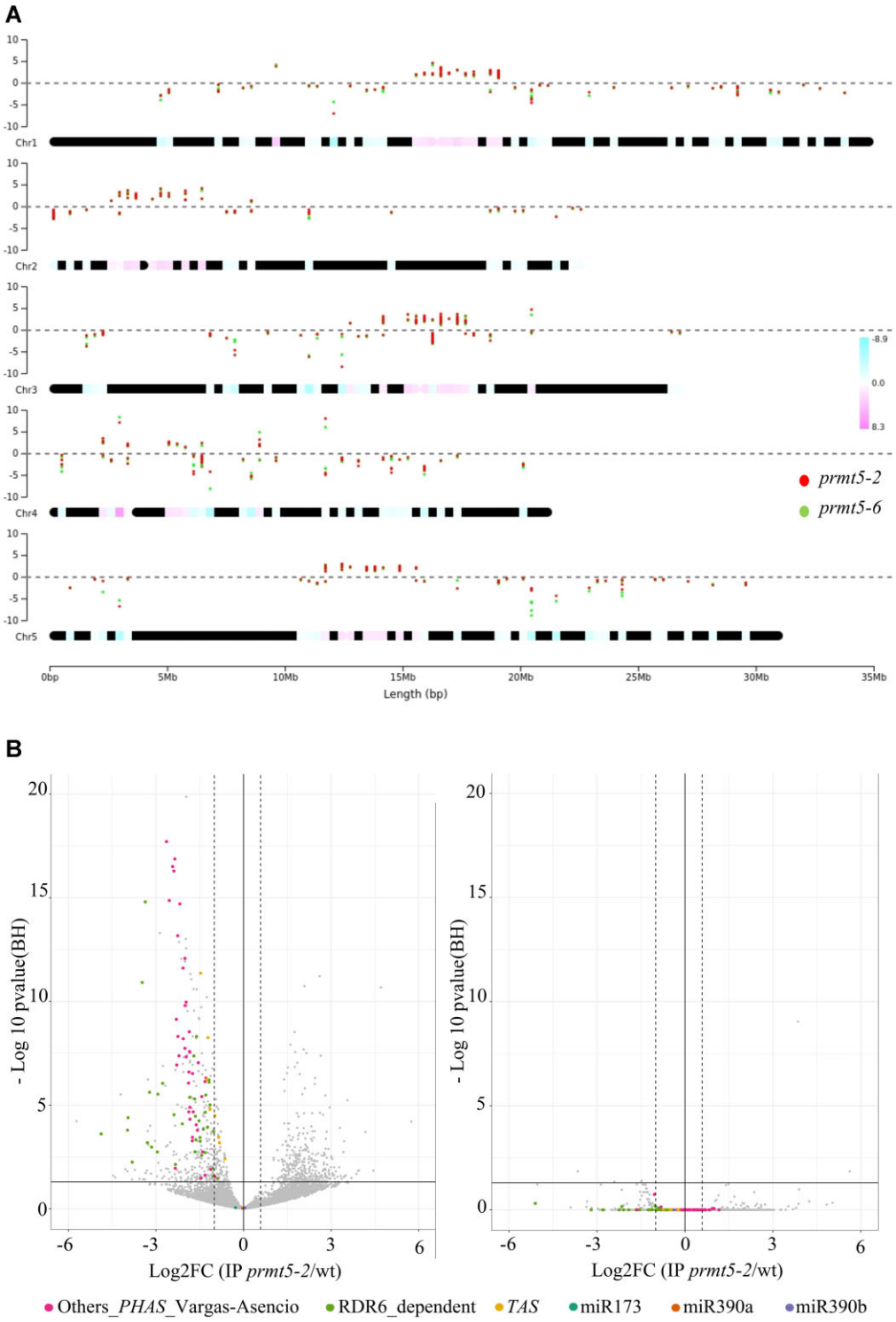

Figure 6. Arginine symmetric dimethylation of AtAGO1 promotes phasiRNA loading in *A. thaliana* buds. (**A**) chromoMap representation combining chromoMap-Scatter Plot and chromoMap-Heatmap to analyse the distribution on chromosomes of all loci producing Differentially Loaded 21 nt-long sRNA (DL-sRNA) for both *atprmt5-2* and *atprmt5-6* mutants compared to wt. The DL-sRNA are mapped to TAIR10 reference genome sliced into successive 100 nt-long windows in each chromosome (x-axis). The centromeres are also represented. Only the 100 bp bin windows with a *P*-value higher than 0.05 are depicted as a chromoMap-Scatter Plot and corresponding Log_2FC (Fold change) are assessed both in the y-axis and as chromosome heatmaps (heat colour scale indicated on right). These selected DL-sRNA are depicted as red and green dots for *atprmt5-2*/wt and *atprmt5-6*/wt respectively. (**B**) Some pools of phasiRNA are less loaded in AtAGO1 in *atprmt5* mutants. At left, volcano-plot depicts all the 100 bp genomic containing DL-sRNA in *atprmt5-2* mutant compared to wt with a *P*-value higher than 0.05. The volcano plot at right shows their level assessed in the input fraction of each IPs. Dots corresponding to siRNA identified as downregulated in *rdr6-11* (RDR6_dependent) in Zheng *et al.* (58); others *PHAS* loci identified by Vargas-Asencio and Perry (2020), and *TAS* loci (*TAS1C TAS3A* and *TAS3B)* and their triggering miRNAs (miR173 and miR390a/b respectively) are coloured.

the silencing effector to the site of piRNA processing (18,19). In the protozoan parasite *Toxoplasma gondii*, TgAGO lacks the catalytic DDE/H triad, and the association of TSN protein to its methylated RGG motifs N-terminal region provides more efficient slicer activity (66). In this work, we have observed an association between AtAGO1 and AtTSN proteins, the only sDMA reader identified so far in plants. Our results suggest that the presence of sDMA marks on AtAGO1 is not strictly required for the association with AtTSN proteins but may rather facilitate or stabilize it. Whether the TSN/AGO1 association observed in the *prmt5* mutant background depends on the remaining aDMA residues or an R-independent mechanism possibly involving another region of AtAGO1 remains an open question. TSN may act as an auxiliary factor that helps to reinforce AGO1 specific actions, as proposed for the Tudor-domain containing factors Krimper and Qin/Kumo with Aub and AGO3, the effectors of the ping-pong pathway in drosophila germlines (67).

The presence of sDMA marks is not essential for AGO1 subcellular trafficking in *A. thaliana*

We have shown that, despite the proximity between RGG/GRR motifs and the NLS (V_2RKRR) within the N-terminal region, the previously reported AtAGO1 nucleocytosolic shuttling activity (22) is not compromised in the *prmt5* mutant grown in standard conditions. Meanwhile, in metazoans, the recognition of sDMA by Tudor proteins triggers the localization of Piwi family (MILI, MIWI, and MIWI2) to the germline nuage cytoplasmic perinuclear condensates in mouse (19,51) and in the silkworm ovarian cells, a defect in the dynamics of the secondary piRNA pathway can trigger the formation of larger AGO3 aggregates until the normal conditions are recovered (68). Knowing that AtTSN proteins are described as docking platforms for stress granules components, we have assessed the impact of the *prmt5* mutation on AtAGO1 subcellular trafficking in the context of abiotic stress. Notably, our work uncovers that, upon heat stress, AtAGO1 can be relocated in discrete cytosolic foci that are reminiscent to stress granules. However, our experiments demonstrate that the loss of sDMA modifications in *A. thaliana* does not abolish the AtAGO1 redistribution in cytoplasmic foci upon HS. Taken together, our assays suggest that PRMT5 is not required to regulate AGO1 intracellular trafficking in *A. thaliana*.

The sDMA-modifications of AtAGO1 facilitate the loading of a panel of phasiRNA

The functional analysis of AtAGO1 protein in the *prmt5* background allowed us to demonstrate that AtAGO1 protein level is not significantly impacted by the lack of sDMA marks. We have also shown that the presence of sDMA modifications is not essential for AtAGO1 miRNA loading and for AtAGO1-dependent *SUL* silencing triggered by the *pSUC2-amiRSUL* construct. Our results are consistent with Xu *et al* who concluded (24) that the first 90 aa of AtAGO1, which includes 8 out of the 9 RGG/GRG motifs, are not required for miRNA association. In fact, we rather underscore a specific role in the regulation of a subset of 21nt-long siRNAs in *prmt5*, mainly originated from genes, and previously identified as phasiRNA (57,58,69). This subset is still loaded in phase in AGO1. So, we suggest that the AGO1-dimeR status does not alter the miRNA-dependent primary cleavage of *PHAS* transcripts in *prmt5*. However, our data indicate that the R-met signatures on AGO1 may provide an information for subsequent steps in the phasiRNA amplification. Related to this, the ping-pong pathway which produces secondary piRNAs in metazoan germlines uses the Tudor/sDMA module to bridge both piRNA-type effectors on the processed RNA (70,71). In particular, Huang and collaborators (2021; 70) have shown that sDMA modifications are not involved in the slicing activity of piRNA effectors in drosophila, but they are rather used as a positive signal promoting the assembly and the transfer of the processed RNA substrate from the loaded DmAub-dimeR to the unloaded DmAGO3.

Based on this scenario, we envision that the sDMA/Tudor module may facilitate directly or indirectly the physical recruitment of the phasiRNA-generating machinery near the methylated AGO1 on the cleaved *PHAS* transcripts fragments. Meanwhile, we cannot exclude that aDMA marks on AGO1 also contribute at some point to the selection of *PHAS* targets and phasiRNA loading.

The precise functions of phasiRNA in plant development and the regulation of their putative mRNA targets remain elusive, except for tasiRNA, the subclass of phasiRNA produced from non-coding loci. However, some observations suggest a role for phasiRNA in plant responses to abiotic stresses (72). As the *Arabidopsis thaliana* genome presents few phasiRNA-generating loci compared to other plant genomes, it would be therefore interesting to address the contribution of these sDMA marks in AGO1 action in other plant species, especially under stress conditions.

PRMT5 specific regulations of AGO proteins activity in *A. thaliana*?

The NTE domain of AtAGO2 has been reported to be modified by PRMT5 enzyme (21), and to interact with TSN proteins through its first 1 to 59 aa region. Nevertheless, sDMA modifications lead to some striking differences in the regulation of AtAGO1 and AtAGO2. In Arabidopsis, the presence of sDMA in AtAGO2 leads *in fine* to lower sRNA loading and can be considered as negative marks. Our observations suggest that PRMT5 action in buds may create a favourable context for the loading of some phasiRNA in AtAGO1, whose production also involves an amplification step by RDR6. This regulation looks like what is observed in metazoan germlines, in which the sDMA marks favour the action of AGO/PIWI effectors. They allow to discriminate between unloaded and loaded state of RNA silencing effectors and are required for piRNA processing and amplification through the ping-pong cycle. The loading of a guide piRNA in Aub triggers a modification of its conformation leading to the exposition of its unstructured N-terminus region which becomes then accessible for PRMT5 enzyme. Subsequent recognition of sDMA-Aub by the Tudor domain containing protein Krimper is then required to assemble with AGO3 in the nuage structure and triggers the amplification of piRNAs through the ping-pong cycle (70).

However, the presence of sDMA and aDMA modifications on the same NTE region of AtAGO1 adds another layer of complexity in this regulation by R-methylation, so far unique in AGO/PIWI family. This dual control reshuffles the cards and implies further investigations to fully understand the contribution of dimethyl/R marks to AGO1 activity.

A role for DiMethyl/R regulation of AtAGO1 in abiotic stress responses?

In this framework, one context to consider will be plant response to unfavourable conditions, as previously shown for AtAGO2 when Arabidopsis is infected by *P. syringae*. Indeed, all our observations suggest a role for R-methylation regulation of AtAGO1 in abiotic stress responses. To test this, it will be essential to get rid of the pleiotropic phenotypes triggered by *atprmt5* mutation that may interfere and mask the identification of specific DiMethyl/R-AGO1 dependent contributions. Thus, it will be essential to produce a version of AtAGO1 depleted of all DiMethyl/R marks to address all these questions in future.

Data availability

All sRNA sequencing data supporting the findings of this study are deposited in the Gene Expression Omnibus under accession code GSE236628. The mass spectrometric data were deposited to the ProteomeXchange Consortium via the PRIDE partner repository with the dataset identifier PXD043460.

Supplementary data

Supplementary Data are available at NAR Online.

Acknowledgements

We thank Dominique Pontier for all discussions, reading of the manuscript, as well as all her support and advice, in particular on RT-qPCR experiments. Natacha Bies-Etheve for all discussions during this project. Claire Picart for microscopy service and Viviane Jean et Christelle Roigt for plant culture service. We also thank Nathalie Giovinazzo and Jean-Luc Gallois for their support and help to quantify leaf chlorosis, Jean-Jacques Favory for providing *pDCP1-YFP-DCP1/pPAB2-RFP-PAB2*/col0 line, Florian Brioudes and Olivier Voinnet for providing the *amiRSUL* line and helpful advices, and finally Nicolas Bologna for providing *pAGO1-GFP-AGO1/ago1-3* seeds and fruitful discussions.

Author Contributions: Study design: J.A.F; mutants characterization and molecular biology: C.B.V, M.L, J.A.F; microscopy analyses: : C.B.V, M.L; Immunoprecipitations and PTM immunodetection: J.A.F; Picture analyses via Image J: C.B.V; sRNA-seq and statistical analyses: M.C.C, C.B.V; mass spectrometry and data post-processing: L.K; writing: J.A.F, C.B.V, T.L and supervision: J.A.F and T.L.

Funding

This study was supported by the Centre National de la Recherche Scientific (CNRS), and by a 'projet central' grant from the 'Laboratoires d'Excellences (LABEX)' TULIP (ANR-10-LABX-41) to J.A.F. C.B.V work was also supported by a Ph.D. grant from the Université de Perpignan *Via Domitia* (Ecole Doctorale Energie et Environnement ED305) and a PhD mobility package from the 'Ecole Universitaire de Recherche (EUR)' TULIP-GS (ANR-18-EURE-0019), and this mobility was done within the framework of a collaboration with GAFL laboratory (INRAE, Avignon, France). The mass spectrometry instrumentation was funded by the University of Strasbourg, IdEx 'Equipement mi-lourd' 2015. The funders had no role in study design, data collection and analysis, decision to publish or preparation of the paper.

Conflicts of interest statement

None declared.

References

1. Pumplin,N. and Voinnet,O. (2013) RNA silencing suppression by plant pathogens: defence, counter-defence and counter-counter-defence. *Nat. Rev. Micro.*, **11**, 745–760.
2. Borges,F. and Martienssen,R.A. (2015) The expanding world of small RNAs in plants. *Nat. Rev. Mol. Cell Biol.*, **16**, 727–741.
3. Waheed,S., Anwar,M., Saleem,M.A., Wu,J., Tayyab,M. and Hu,Z. (2021) The critical role of small RNAs in regulating plant innate immunity. *Biomolecules*, **11**, 184.
4. Lopez-Gomollon,S. and Baulcombe,D.C. (2022) Roles of RNA silencing in viral and non-viral plant immunity and in the crosstalk between disease resistance systems. *Nat. Rev. Mol. Cell Biol.***23**, 645–662.
5. Morel,J.B., Godon,C., Mourrain,P., Béclin,C., Boutet,S., Feuerbach,F., Proux,F. and Vaucheret,H. (2002) Fertile hypomorphic ARGONAUTE (ago1) mutants impaired in post-transcriptional gene silencing and virus resistance. *Plant Cell*, **14**, 629–639.
6. Carbonell,A. and Carrington,J.C. (2015) Antiviral roles of plant ARGONAUTES. *Curr. Opin. Plant Biol.*, **27**, 111–117.
7. Mason,G.A., Lemus,T. and Queitsch,C. (2016) The mechanistic underpinnings of an ago1-mediated, environmentally dependent, and stochastic phenotype. *Plant Physiol.*, **170**, 2420–2431.
8. Pegler,J.L., Oultram,J.M.J., Grof,C.P.L. and Eamens,A.L. (2019) Profiling the abiotic stress responsive microRNA landscape of arabidopsis thaliana. *Plants (Basel)*, **8**, 58.
9. Bohmert,K., Camus,I., Bellini,C., Bouchez,D., Caboche,M. and Benning,C. (1998) AGO1 defines a novel locus of Arabidopsis controlling leaf development. *EMBO J.*, **17**, 170–180.
10. Vaucheret,H., Vazquez,F., Crété,P. and Bartel,D.P. (2004) The action of ARGONAUTE1 in the miRNA pathway and its regulation by the miRNA pathway are crucial for plant development. *Genes Dev.*, **18**, 1187–1197.
11. Vaucheret,H., Mallory,A.C. and Bartel,D.P. (2006) AGO1 homeostasis entails coexpression of MIR168 and AGO1 and preferential stabilization of miR168 by AGO1. *Mol. Cell*, **22**, 129–136.
12. Du,F., Gong,W., Boscá,S., Tucker,M., Vaucheret,H. and Laux,T. (2019) Dose-dependent AGO1-mediated inhibition of the miRNA165/166 pathway modulates stem cell maintenance in Arabidopsis shoot apical meristem. *Plant Commun.*, **1**, 100002.
13. Dalmadi,Á., Miloro,F., Bálint,J., Várallyay,É. and Havelda,Z. (2021) Controlled RISC loading efficiency of miR168 defined by miRNA duplex structure adjusts ARGONAUTE1 homeostasis. *Nucleic Acids Res.*, **49**, 12912–12928.
14. Earley,K., Smith,M., Weber,R., Gregory,B. and Poethig,R. (2010) An endogenous F-box protein regulates ARGONAUTE1 in Arabidopsis thaliana. *Silence*, **1**, 15.
15. Derrien,B. and Genschik,P. (2014) When RNA and protein degradation pathways meet. *Front. Plant Sci.*, **5**. 161.
16. Hacquard,T., Clavel,M., Baldrich,P., Lechner,E., Pérez-Salamó,I., Schepetilnikov,M., Derrien,B., Dubois,M., Hammann,P., Kuhn,L., *et al.* (2022) The Arabidopsis F-box protein FBW2 targets AGO1 for degradation to prevent spurious loading of illegitimate small RNA. *Cell Rep.*, **39**, 110671.
17. Bressendorff,S., Kausika,S., Zobbe Sjøgaard,I.M., Oksbjerg,E., Michels,A., Poulsen,C. and Brodersen,P. (2023) The N-coil and the globular N-terminal domain of plant ARGONAUTE1 are interaction hubs for regulatory factors. *Biochem. J.*, **480**, 957–974.

18. Kirino,Y., Kim,N., de Planell-Saguer,M., Khandros,E., Chiorean,S., Klein,P.S., Rigoutsos,I., Jongens,T.A. and Mourelatos,Z. (2009) Arginine methylation of Piwi proteins catalysed by dPRMT5 is required for Ago3 and Aub stability. *Nat. Cell Biol.*, **11**, 652–658.
19. Nishida,K.M., Okada,T.N., Kawamura,T., Mituyama,T., Kawamura,Y., Inagaki,S., Huang,H., Chen,D., Kodama,T., Siomi,H., *et al.* (2009) Functional involvement of Tudor and dPRMT5 in the piRNA processing pathway in Drosophila germlines. *EMBO J.*, **28**, 3820–3831.
20. Vagin,V.V., Wohlschlegel,J., Qu,J., Jonsson,Z., Huang,X., Chuma,S., Girard,A., Sachidanandam,R., Hannon,G.J. and Aravin,A.A. (2009) Proteomic analysis of murine Piwi proteins reveals a role for arginine methylation in specifying interaction with Tudor family members. *Genes Dev.*, **23**, 1749–1762.
21. Hu,P., Zhao,H., Zhu,P., Xiao,Y., Miao,W., Wang,Y. and Jin,H. (2019) Dual regulation of Arabidopsis AGO2 by arginine methylation. *Nat. Commun.*, **10**, 844.
22. Bologna,N.G., Iselin,R., Abriata,L.A., Sarazin,A., Pumplin,N., Jay,F., Grentzinger,T., Dal Peraro,M. and Voinnet,O. (2018) Nucleo-cytosolic shuttling of ARGONAUTE1 prompts a revised model of the plant MicroRNA pathway. *Mol. Cell*, **69**, 709–719.e5.
23. Poulsen,C., Vaucheret,H. and Brodersen,P. (2013) Lessons on RNA silencing mechanisms in plants from eukaryotic argonaute structures. *Plant Cell*, **25**, 22–37.
24. Xu,Y., Zhang,Y., Li,Z., Soloria,A.K., Potter,S. and Chen,X. (2023) The N-terminal extension of Arabidopsis ARGONAUTE 1 is essential for microRNA activities. *PLoS Genet.*, **19**, e1010450.
25. Brioudes,F., Jay,F., Sarazin,A., Grentzinger,T., Devers,E.A. and Voinnet,O. (2021) HASTY, the Arabidopsis EXPORTIN5 ortholog, regulates cell-to-cell and vascular microRNA movement. *EMBO J.*, **40**, e107455.
26. Varadi,M., Anyango,S., Deshpande,M., Nair,S., Natassia,C., Yordanova,G., Yuan,D., Stroe,O., Wood,G., Laydon,A., *et al.* (2022) AlphaFold Protein Structure Database: massively expanding the structural coverage of protein-sequence space with high-accuracy models. *Nucleic Acids Res.*, **50**, D439–D444.
27. Hurkman,W.J. and Tanaka,C.K. (1986) Solubilization of plant membrane proteins for analysis by two-dimensional gel electrophoresis. *Plant Physiol.*, **81**, 802–806.
28. Bouyssié,D., Hesse,A.M., Mouton-Barbosa,E., Rompais,M., Macron,C., Carapito,C., Gonzalez de Peredo,A., Couté,Y., Dupierris,V., Burel,A., *et al.* (2020) Proline: an efficient and user-friendly software suite for large-scale proteomics. *Bioinformatics*, **36**, 3148–3155.
29. Bolger,A.M., Lohse,M. and Usadel,B. (2014) Trimmomatic: a flexible trimmer for Illumina sequence data. *Bioinformatics*, **30**, 2114–2120.
30. Love,M.I., Huber,W. and Anders,S. (2014) Moderated estimation of fold change and dispersion for RNA-seq data with DESeq2. *Genome Biol.*, **15**, 550.
31. Anand,L. and Rodriguez Lopez,C.M. (2022) ChromoMap: an R package for interactive visualization of multi-omics data and annotation of chromosomes. *BMC Bioinf.*, **23**, 33.
32. De Paoli,E., Dorantes-Acosta,A., Zhai,J., Accerbi,M., Jeong,D.H., Park,S., Meyers,B.C., Jorgensen,R.A. and Green,P.J. (2009) Distinct extremely abundant siRNAs associated with cosuppression in petunia. *RNA*, **15**, 1965–1970.
33. Musiani,D., Bok,J., Massignani,E., Wu,L., Tabaglio,T., Ippolito,M.R., Cuomo,A., Ozbek,U., Zorgati,H., Ghoshdastider,U., *et al.* (2019) Proteomics profiling of arginine methylation defines PRMT5 substrate specificity. *Sci. Signal*, **12**, eaat8388.
34. Pei,Y., Niu,L., Lu,F., Liu,C., Zhai,J., Kong,X. and Cao,X. (2007) Mutations in the type II protein arginine methyltransferase AtPRMT5 result in pleiotropic developmental defects in Arabidopsis. *Plant Physiol.*, **144**, 1913–1923.
35. Kidner,C.A. and Martienssen,R.A. (2005) The role of ARGONAUTE1 (AGO1) in meristem formation and identity. *Dev. Biol.*, **280**, 504–517.
36. Wang,X., Zhang,Y., Ma,Q., Zhang,Z., Xue,Y., Bao,S. and Chong,K. (2007) SKB1-mediated symmetric dimethylation of histone H4R3 controls flowering time in Arabidopsis. *EMBO J.*, **26**, 1934–1941.
37. Yue,M., Li,Q., Zhang,Z.Y., Zhang,Z. and Bao,S. (2013) Histone H4R3 methylation catalyzed by SKB1/PRMT5 is required for maintaining shoot apical meristem. *PLoS One*, **8**, e83258.
38. Liu,H., Wang,J.Y., Huang,Y., Li,Z., Gong,W., Lehmann,R. and Xu,R.M. (2010) Structural basis for methylarginine-dependent recognition of Aubergine by Tudor. *Genes Dev.*, **24**, 1876–1881.
39. Chen,C., Nott,T.J., Jin,J. and Pawson,T. (2011) Deciphering arginine methylation: tudor tells the tale. *Nat. Rev. Mol. Cell Biol.*, **12**, 629–642.
40. Gayatri,S. and Bedford,M.T. (2014) Readers of histone methylarginine marks. *Biochim. Biophys. Acta*, **1839**, 702–710
41. Thomson,T. and Lasko,P. (2005) Tudor and its domains: germ cell formation from a Tudor perspective. *Cell Res.*, **15**, 281–291.
42. Pek,J.W., Anand,A. and Kai,T. (2012) Tudor domain proteins in development. *Development*, **139**, 2255–2266.
43. Ying,M. and Chen,D. (2012) Tudor domain-containing proteins of drosophila melanogaster. *Dev. Growth Differ.*, **54**, 32–43.
44. Liu,K., Chen,C., Guo,Y., Lam,R., Bian,C., Xu,C., Zhao,D.Y., Jin,J., MacKenzie,F., Pawson,T., *et al.* (2010) Structural basis for recognition of arginine methylated Piwi proteins by the extended Tudor domain. *Proc. Natl. Acad Sci. U.S.A.*, **107**, 18398–18403.
45. Gan,B., Chen,S., Liu,H., Min,J. and Liu,K. (2019) Structure and function of eTudor domain containing TDRD proteins. *Crit. Rev. Biochem. Mol. Biol.*, **54**, 119–132.
46. Ku,H.Y., Gangaraju,V.K., Qi,H., Liu,N. and Lin,H. (2016) Tudor-SN interacts with Piwi antagonistically in regulating spermatogenesis but synergistically in silencing transposons in Drosophila. *PLoS Genet.*, **12**, e1005813.
47. Frei dit Frey,N., Muller,P., Jammes,F., Kizis,D., Leung,J., Perrot-Rechenmann,C. and Bianchi,M.W. (2010) The RNA binding protein Tudor-SN is essential for stress tolerance and stabilizes levels of stress-responsive mRNAs encoding secreted proteins in Arabidopsis. *Plant Cell*, **22**, 1575–1591.
48. Azevedo,J., Cooke,R. and Lagrange,T. (2011) Taking RISCs with ago hookers. *Curr. Opin. Plant Biol.*, **14**, 594–600.
49. Garcia,D., Garcia,S., Pontier,D., Marchais,A., Renou,J.P., Lagrange,T. and Voinnet,O. (2012) Ago hook and RNA helicase motifs underpin dual roles for SDE3 in antiviral defense and silencing of nonconserved intergenic regions. *Mol. Cell*, **48**, 109–120.
50. Kirino,Y., Vourekas,A., Sayed,N., de Lima Alves,F., Thomson,T., Lasko,P., Rappsilber,J., Jongens,T.A. and Mourelatos,Z. (2010) Arginine methylation of aubergine mediates Tudor binding and germ plasm localization. *RNA*, **16**, 70–78.
51. Arkov,A.L. and Ramos,A. (2010) Building RNA-protein granules: insight from the germline. *Trends Cell Biol.*, **20**, 482–490.
52. Courchaine,E.M., Barentine,A.E.S., Straube,K., Lee,D.R., Bewersdorf,J. and Neugebauer,K.M. (2021) DMA-tudor interaction modules control the specificity of in vivo condensates. *Cell*, **184**, 3612–3625.
53. Lim,L.X., Isshiki,W., Iki,T., Kawaguchi,S. and Kai,T. (2022) The Tudor domain-containing protein, Kotsubu (CG9925), localizes to the nuage and functions in piRNA. *Biogenesis in D. Melanogaster. Front. Mol. Biosci.*, **9**, 818302.
54. Hofweber,M., Hutten,S., Bourgeois,B., Spreitzer,E., Niedner-Boblenz,A., Schifferer,M., Ruepp,M.D., Simons,M., Niessing,D., Madl,T., *et al.* (2018) Phase separation of FUS is suppressed by its nuclear import receptor and arginine methylation. *Cell*, **173**, 706–719.
55. Gutierrez-Beltran,E., Moschou,P.N., Smertenko,A.P. and Bozhkov,P.V. (2015) Tudor staphylococcal nuclease links formation of stress granules and processing bodies with mRNA catabolism in Arabidopsis. *Plant Cell*, **27**, 926–943.
56. Gutierrez-Beltran,E., Elander,P.H., Dalman,K., Dayhoff,G.W., Moschou,P.N., Uversky,V.N., Crespo,J.L. and Bozhkov,P.V. (2021) Tudor staphylococcal nuclease is a docking platform for stress

granule components and is essential for SnRK1 activation in Arabidopsis. *EMBO J.*, **40**, e105043.
57. Vargas-Asencio,J.A. and Perry,K.L. (2020) A small RNA-mediated regulatory network in Arabidopsis thaliana demonstrates connectivity between phasiRNA regulatory modules and extensive Co-regulation of transcription by miRNAs and phasiRNAs. *Front. Plant Sci.*, **10**, 1710.
58. Zheng,Q., Ryvkin,P., Li,F., Dragomir,I., *et al.* (2010) Genome-wide double-stranded RNA sequencing reveals the functional significance of base-paired RNAs in Arabidopsis. *PLoS Genet.*, **6**, e1001141
59. Zheng,S., Moehlenbrink,J., Lu,Y.C., Zalmas,L.P., Sagum,C.A., Carr,S., McGouran,J.F., Alexander,L., Fedorov,O., Munro,S., *et al.* (2013) Arginine methylation-dependent reader-writer interplay governs growth control by E2F-1. *Mol. Cell*, **52**, 37–51.
60. Li,M., An,W., Xu,L., Lin,Y., Su,L. and Liu,X. (2019) The arginine methyltransferase PRMT5 and PRMT1 distinctly regulate the degradation of anti-apoptotic protein $CFLAR_L$ in human lung cancer cells. *J. Exp. Clin. Cancer Res.*, **38**, 64.
61. Guccione,E., Bassi,C., Casadio,F., Martinato,F., Cesaroni,M., Schuchlautz,H., Lüscher,B. and Amati,B. (2007) Methylation of histone H3R2 by PRMT6 and H3K4 by an MLL complex are mutually exclusive. *Nature*, **449**, 933–937.
62. Migliori,V., Müller,J., Phalke,S., Low,D., Bezzi,M., Mok,W.C., Sahu,S.K., Gunaratne,J., Capasso,P., Bassi,C., *et al.* (2012) Symmetric dimethylation of H3R2 is a newly identified histone mark that supports euchromatin maintenance. *Nat. Struct. Mol. Biol.*, **19**, 136–144.
63. Chittka,A. (2010) Dynamic distribution of histone H4 arginine 3 methylation marks in the developing murine cortex. *PLoS One*, **5**, e13807.
64. Yan,D., Zhang,Y., Niu,L., Yuan,Y. and Cao,X. (2007) Identification and characterization of two closely related histone H4 arginine 3 methyltransferases in Arabidopsis thaliana. *Biochem. J.*, **408**, 113–121.
65. Dhar,S., Vemulapalli,V., Patananan,A.N., Huang,G.L., Di Lorenzo,A., Richard,S., Comb,M.J., Guo,A., Clarke,S.G. and Bedford,M.T. (2013) Loss of the major type I arginine methyltransferase PRMT1 causes substrate scavenging by other. *PRMTs. Sci Rep.*, **3**, 1311.
66. Musiyenko,A., Majumdar,T., Andrews,J., Adams,B. and Barik,S. (2012) PRMT1 methylates the single Argonaute of Toxoplasma gondii and is important for the recruitment of Tudor nuclease for target RNA cleavage by antisense guide RNA. *Cell. Microbiol.*, **14**, 882–901.
67. Sato,K., Iwasaki,Y.W., Siomi,H. and Siomi,M.C. (2015) Tudor-domain containing proteins act to make the piRNA pathways more robust in Drosophila. *Fly (Austin)*, **9**, 86–90.
68. Nishida,K.M., Sakakibara,K., Sumiyoshi,T., Yamazaki,H., Mannen,T., Kawamura,T., Kodama,T. and Siomi,M.C. (2020) Siwi levels reversibly regulate secondary piRISC biogenesis by affecting Ago3 body morphology in Bombyx mori. *EMBO J.*, **39**, e105130.
69. Si-Ammour,A., Windels,D., Arn-Bouldoires,E., Kutter,C., Ailhas,J., Meins,F. Jr and Vazquez,F. (2011) miR393 and secondary siRNAs regulate expression of the TIR1/AFB2 auxin receptor clade and auxin-related development of Arabidopsis leaves. *Plant Physiol.*, **157**, 683–691.
70. Huang,X., Hu,H., Webster,A., Zou,F., Du,J., Patel,D.J., Sachidanandam,R., Toth,K.F., Aravin,A.A. and Li,S. (2021) Binding of guide piRNA triggers methylation of the unstructured N-terminal region of Aub leading to assembly of the piRNA amplification complex. *Nat. Commun.*, **12**, 4061.
71. Bronkhorst,A.W., Lee,C.Y., Möckel,M.M., Ruegenberg,S., de,J., Domingues,A.M., Sadouki,S., Piccinno,R., Sumiyoshi,T., Siomi,M.C., *et al.* (2023) An extended Tudor domain within Vreteno interconnects Gtsf1L and Ago3 for piRNA biogenesis in Bombyx mori. *EMBO J.*, e114072.
72. Liu,Y., Teng,C., Xia,R. and Meyers,B.C. (2020) PhasiRNAs in plants: their biogenesis, genic sources, and roles in stress responses, development, and reproduction. *Plant Cell*, **32**, 3059–3080.
73. Gibson,L.C., Marrison,J.L., Leech,R.M., Jensen,P.E., Bassham,D.C., Gibson,M. and Hunter,C.N. (1996) A putative Mg chelatase subunit from Arabidopsis thaliana cv C24. Sequence and transcript analysis of the gene, import of the protein into chloroplasts, and in situ localization of the transcript and protein. *Plant Physiol.*, **111**, 61–71.

Received: July 6, 2023. **Revised:** December 18, 2023. **Editorial Decision:** January 5, 2024. **Accepted:** January 12, 2024